The influence of physical and spatial substrate characteristics on endothelial cells

Oddny Bjorgvinsdottir [c], Stephen J. Ferguson [a], Bergthora Sigridur Snorradottir [c], Thorarinn Gudjonsson [d], Karin Wuertz-Kozak [b,*]

[a] Institute for Biomechanics, ETH Zurich, Gloriastrasse 37 / 39, 8092, Zurich, Switzerland
[b] Department of Biomedical Engineering, Rochester Institute of Technology (RIT), 160 Lomb Memorial Drive Bldg. 73, Rochester, NY, 14623, USA
[c] Faculty of Pharmaceutical Sciences, University of Iceland, Hofsvallagata 53, 107 Reykjavik, Iceland
[d] Faculty of Medicine, University of Iceland, Vatnsmyrarvegur 16, 101 Reykjavik, Iceland

ABSTRACT

Cardiovascular diseases are a main cause of death worldwide, leading to a growing demand for medical devices to treat this patient group. Central to the engineering of such devices is a good understanding of the biology and physics of cell-surface interactions. In existing blood-contacting devices, such as vascular grafts, the interaction between blood, cells, and material is one of the main limiting factors for their long-term durability. An improved understanding of the material's chemical- and physical properties as well as its structure all play a role in how endothelial cells interact with the material surface. This review provides an overview of how different surface structures influence endothelial cell responses and what is currently known about the underlying mechanisms that guide this behavior. The structures reviewed include decellularized matrices, electrospun fibers, pillars, pits, and grated surfaces.

1. Introduction

Topography, or the study and description of physical features of an area, is a key concept for the design of any cellular scaffold. It can be defined by surface orientation and roughness and is characterized by a succession of peaks and valleys. Understanding how scaffold features affect endothelial cell behavior is of the utmost importance for the design of various blood contacting devices. The need is clear as cardiovascular diseases are the leading cause of death worldwide and accounts for the death of over on third of the global population [1]. Current treatment options to improve or restore the function of the diseased tissue include medication, the use of implants or biomedical devices, and transplantation [2]. With the increasing use of blood contacting devices including implantable devices, such as transcatheter valves and ventricular assist devices, it is necessary to tackle issues specific to these blood-contacting devices. These issues arise when blood is in contact with an artificial material. The interaction results in thrombosis, the formation of thrombus, or blood clots in blood-carrying cavities. This phenomenon is a common problem for blood-contacting

devices. It negatively effects the clinical outcomes by causing malfunction or failure of devices and can cause severe complications for the patient [3]. Thrombi formation is influenced by several factors such as internal shear stress, infection, inadequate anticoagulation, and the choice of device material. The underlying mechanism is a complex interplay of protein adsorption, adhesion of platelets, leukocytes, red blood cells, thrombin generation, and complement activation [4].

Bio-engineered methods to prevent thrombosis in blood-contacting medical devices have mainly focused on synthesizing less thrombogenic surfaces or controlling the risk through medication. Attempts to reduce the thrombogenic properties of the materials have aimed at either inhibiting protein and cell adsorption or thrombin generation and fibrin formation [4]. Even in state-of-the-art device surfaces with heparin coatings, a concurrent, systemic administration of antiplatelet agents and/or anticoagulants is still necessary to ensure effectiveness [5]. Fine-tuning the administered drug can be critical to effectively prevent thrombosis and avoid bleeding complications, both of which can be life threatening to the patient.

In comparison, intact endothelium is naturally anti-thrombogenic

* Corresponding author.
E-mail addresses: odb9@hi.is (O. Bjorgvinsdottir), sferguson@ethz.ch (S.J. Ferguson), bss@hi.is (B.S. Snorradottir), tgudons@hi.is (T. Gudjonsson), kwbme@rit.edu (K. Wuertz-Kozak).

through the expression of antiplatelet agents and anticoagulant agents that prevent platelet aggregation and fibrin formation. However, in the case of damaged or dysfunctional endothelium, the cells trigger fibrin formation, as well as platelet adhesion and aggregation. Finally, endothelial cells release pro-fibrinolytic agents in the case of damage that initiate fibrinolysis to degrade the clot. A healthy and functional endothelium is thus essential for maintaining hemostasis and preventing thrombosis [6].

Besides advances in anti-platelet and anticoagulant therapies and developing less thrombogenic material surfaces, research efforts have also focused on creating endothelialized surfaces. If a healthy endothelialized surface could be obtained in such a hybrid system, it would have the potential to fully prevent thrombi to obviate the need for systemic antithrombotic therapy. Research on endothelialized substrates for blood-contacting devices has developed substantially over the last decades, with a special focus on stents and vascular grafts [7,8]. Despite reaching clinical trials, the results have been less than optimal.

It is currently known that the interaction of the endothelium with the underlying substrate is a combination of physical, chemical, and mechanical factors. These include, for example, the extracellular matrix structure, binding of cytoactive factors into that matrix and stiffness [[9–11]. Cytoactive factors include molecules, typically proteins or peptides, that exert specific effects on cells, influencing their behavior, function, or development. These factors can regulate processes such as cell growth, differentiation, migration, and survival through interactions with cell surface receptors or intracellular signaling pathways. While growth factors, cytokines, and chemokines are the most classical representatives, the group also encompasses other functional molecules, such as hormones, neurotransmitters, and ECM components. The overall surface topography of the material has an effect on the expression of over 3000 genes in Human Umbilical Vein Endothelial cells (HUVECs) [12]. It also has a direct impact on the adhesion, proliferation, migration, morphology, and phenotype of endothelial cells [13–21]. Its link to inflammation is also of great importance for the function of vascular devices as EC morphology regulates inflammatory cells and affects their cytokine and chemokine secretion [22,23]. It can also have an anti-inflammatory effect on the endothelial cells themselves, an important effect that has the potential to improve the performance of such substrates in vivo [24]. An improved understanding of endothelial function, its interaction with the extracellular environment
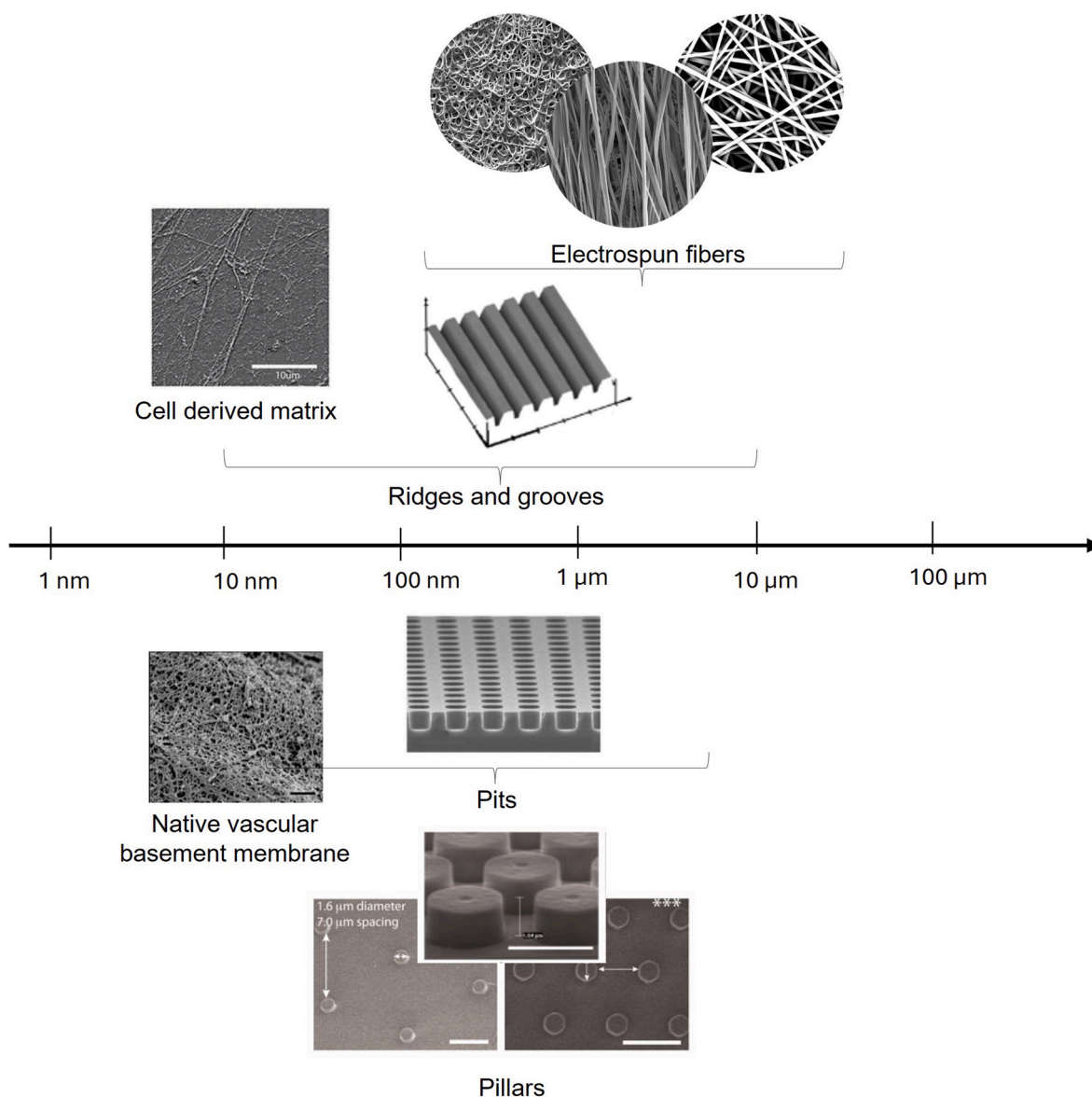

Fig. 1. Topographical features of engineered substrates reivewed compared to the native vascular basement membrane. Figs. reprinted with permission from Refs [39,73,134,147,164].

and synthetic materials will lead to improved strategies for the treatment of vascular diseases.

This review is an overview of how different surface structures influence endothelial cell behavior. Previous reviews have focused more broadly on mammalian cell response to different topographies. However, for an effective design of vascular medical devices, the specific endothelial cellular response is of essence. Here the most common substates used for endothelialization, or the study there of, are reviewed. This includes decellularized matrices, electrospun fibers, pillars, pits, and grated surfaces (see Figs. 1 and 2). Substrates currently used in medical devices on the market are excluded. Even though the general features of these substrates are available, then the more detailed topography of these substrates are not publicly available due to trade secrets. For comparison to the native matrix, "vascular basement membrane" was a key search term but as the vascular basement membrane of various tissue hold specific name, anatomical sites relevant to the engineering like saphenous vein, valve, heart were also included.

2. Vascular basement membranes in the healthy human body

2.1. The endothelium and its extracellular matrix

The cardiovascular system, consisting of the heart, blood vessels and contained blood, plays a multifunctional role in the human body. The endothelium is a monolayer of endothelial cells that forms a single cell layer that lines the interior surface of the entire vascular system. Its role is maintaining vascular homeostasis by regulating the vascular tone and blood fluidity, filtrating fluids, platelet aggregation, inflammation, angiogenesis and to transport various substances throughout the body. It

also plays a major role in immune regulation, inflammation and as a metabolizing and endocrine organ [25–27]. Two of these important and intertwined processes are hemostasis, the physiological process that stops bleeding at the site of an injury and the otherwise anti-thrombogenic function of the cardiovascular system to maintain normal blood flow [28]. These two functions interact with each other and are maintained, to a large extent, by the endothelium, either by secreting factors that promote coagulation or factors that prevent clotting and platelet aggregation [29–31]. The endothelium is part of the vessel wall, which in larger vessels consist of three distinct layers: tunica intima, tunica media and tunica externa [32]. The innermost layer, tunica intima, is comprised of an endothelium that is in contact with blood, basal lamina and a layer of loose connective tissue. The middle layer, tunica media, is mainly composed of smooth muscle cells, elastin and collagen. The outer layer, tunica externa, is a connective tissue, mainly composed of fibroblasts and its connective tissue [33]. Even though the distinct layers all have their unique function and work together as a unit, the most relevant part for the medical industry is the tunica intima because it supports the endothelial cell layer that is in direct contact with the blood.

In large or elastic arteries, the tunica intima layer is composed of endothelial cells, its basement membrane, also known as basal lamina, and subendothelial layer, or internal elastic membrane [34]. The endothelial cells, which synthesize and maintain the basal lamina, are elongated in shape, and are joined by tight junctions (zonulae occuludentes) and gap junctions. Basolateral to the basal lamina is the sub-endothelial stroma, composed of low numbers of fibrocytes and smooth muscles, elastic fibers and a small amount of collagen [35]. The tunica intima is finally separated from the tunica media by a thin layer of
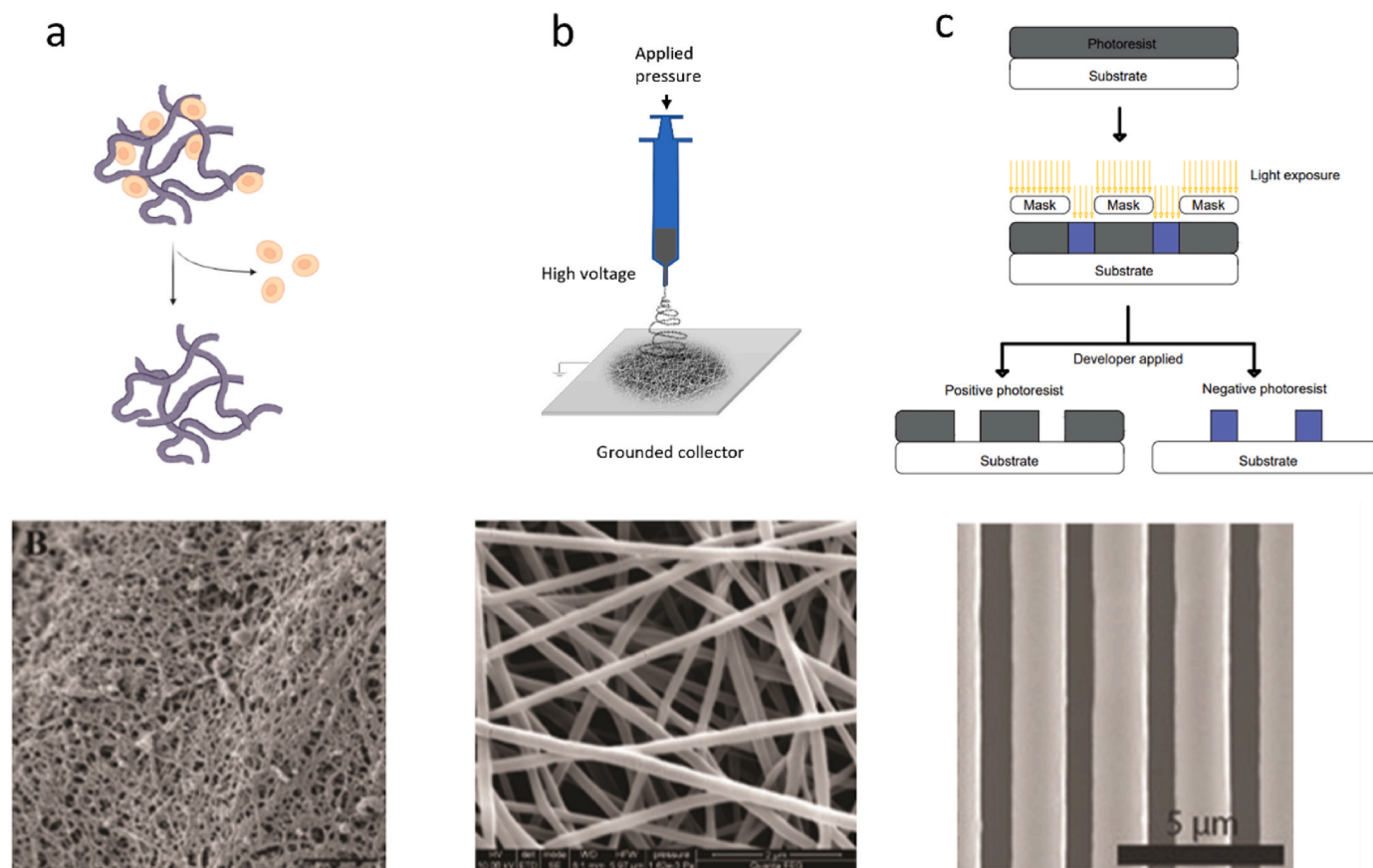

Fig. 2. Conceptual figure illustrating the different approaches reviewed. A. Native aorta basement membrane from Rhesus macaque (scale bar = 600 nm). SEM image reprinted with permission from Ref. [39]. B. Electrospun polycaprolactone fibers (scale bar = 2 μm). C. Grated substrate. SEM image reprinted with permission from Ref. [70].

elastic tissue called the internal elastic lamina [36].

Basement membranes are the main extracellular matrix (ECM) structures found in the vessel wall, underlying the endothelium. Capable of mediating information exchange between the endothelial cells and other surrounding cells, the basement membrane modulates processes including *trans*-membrane molecular diffusion, cell migration, attachment, differentiation, and angiogenesis. It additionally plays an important role in hemostasis. For that purpose, the ECM works via its chemotactic, haptotactic, and opsonic properties [37].

2.2. Structure and function of the vascular basal lamina

In the cardiovascular system, ECMs are part of all blood vessels and are critical for all aspects of vascular biology. The basement membrane is a dense interconnected network composed of about 50 different proteins [38,39]. The major components of the basement membrane are collagen type IV (comprising 50 % of it), laminins (mainly laminin α4 and α5 chains), heparan-sulfate proteoglycans, and nidogens 1 and 2 [38,40–42]. Other minor components of the base membrane include collagens XV and XVIII, SPARC/BM-40/osteopontin, and fibulins [43–46]. The components of the ECM are secreted by endothelial cells and form a connected layer by self-assembly, a process driven by cell-surface anchors and receptors [47,48].

Vascular endothelial cells anchor to, and interact with, the basement membrane and ECM through focal adhesions, composed of integrin, talin, vinculin, α-actinin, and other proteins [39,49]. While several mechanisms may be involved, the formation and maintenance of the focal adhesions is regulated by Rho and the corresponding signaling cascade [49,50].

The topographical features of the matrix, such as the fibers and pores, are in the nanometer range. Matrices from different anatomical sites and species have feature sizes that are reported to be between 30 and 100 nm [11,13,39,51]. The thickness of the membrane itself is also in the nanometer range but can vary depending on the origin of the vessel. In rhesus macaque, the thickness of the basement membranes is 506 ± 14 nm in the aorta, but is thinner in both the carotid artery (319 ± 14 nm) and in the inferior vena cava (286 ± 8.2 nm) [39]. The membrane may increase in thickness with age and disease [52–55].

2.3. Physical and mechanical properties of vascular base membrane

All cells depend on physical extracellular signals to control their functions and to respond to changes in the environment. In vascular engineering, understanding the physical environment experienced by endothelial cells is of great importance to steer cell behavior on implantable devices. Although the physical environment should be an important input in biomedical design, these properties have not been studied and described in detail. The existing literature describes the ultrastructure of basement membranes in general. Fewer describe this matrix specifically for the cardiovascular system. The matrix is mainly described with histology images and do not quantify the physical aspects in detail.

The composition of the vascular extracellular matrix and therefore their physical properties differ between anatomical sites. These structural differences are likely due to the specialized function of these tissues. The complex topographical features of various anatomical sites have been characterized to a certain extent by scanning electron microscopy, atomic force microscopy, and transmission electron microscopy. These studies have given valuable information about the surface roughness, fibers thickness, pore size, and mechanical properties.

The feature dimensions of the human corneal basement membrane, the Descemet's membrane, heart valve matrix and the saphenous vein are summarized in Table 1.

Determination of the mechanical properties of the vascular basement membrane have so far been based on whole vascular tissues (Table 2). Even though the measurements of isolated tissue would give the exact

Table 1

Topographical feature of vascular basement membranes [nm].

Tissue type	Method	Elevation	Fibers	Pores
Human corneal basement membrane[a]	SEM	182 ± 49	46 ± 16	92 ± 34
	TEM	165 ± 78	–	–
	AFM	243 ± 34	–	–
Human Descemet's membrane[a]	SEM	131 ± 41	38 ± 15	31 ± 9
	TEM	107 ± 50	–	–
	AFM	186 ± 45	–	–
Porcine aortic heart valve (ventricular BM)[b]	SEM	26 ± 13	28 ± 3	32 ± 2
Porcine aortic heart valve (fibrosal BM)[b]	SEM	22 ± 11	30 ± 2	28 ± 4
Rhesus macaque aorta[c]	SEM	–	31 ± 1	59 ± 5
Rhesus macaque carotid[c]	SEM	–	30 ± 2	63 ± 6
Rhesus macaque saphenous[c]	SEM	–	27 ± 1	38 ± 2

BM: basement membranes; SEM: scanning electron microscope; TEM: transmission electron microscope; AFM: atomic force microscope; -: not available. Values adopted from a [51], b [13], c [39].

Table 2

Mechanical properties of vascular tissue.

Young's modulus	Type of tissue	Method	Comments	Ref
8.2 ± 3.8 kPa	Human greater saphenous vein	Microindentation	The endothelial side of a human greater saphenous vein was measured	[56]
547.5 kPa	Porcine aorta	Nanoindentation	Young's modulus derived from the reduced modulus. Poisson ratio assumed to be 0.5 Tissue excised within 1h of death and tested within 1 week of excision Stored in saline at 5 °C or on ice before testing	[57]
69.0 ± 12.8 kPa	Small-caliber porcine artery	Tactile mapping system	The elastin-rich region of the lamina elastica interna was measured Samples stored at −20 °C until use	[58]
34.3 kPa	Healthy human femoral artery	AFM-based indentation		[59]
5–8 kPa	Carotid arteries	AFM indentation	Tissue excised from 6 months old pigs Young's modulus of arterial media was measured	[60]

stiffness, the stiffness of the matrix is generally thought to correspond to the stiffness of the tissue [61]. Few studies have investigated the isolated basement membrane, but only from the eye (Table 3). For the different types of matrices and tissues, the Young's moduli have been reported to be in the range of 5 kPa - 4 MPa.

Regardless of tissue type, fibrillar collagens, mainly types I, II, and III provide tensile strength and stiffness [51]. Studies of mechanical behavior of individual matrix proteins have been limited to collagen I, fibrin, and fibronectin that are available in large quantities and therefore cost-effective to study [61]. Similar work has not been done with proteins more abundant in the vascular wall, like type IV collagens or laminins, but these are, without a doubt, the components of greatest importance. It is however known that cell-free fibrin and collagen fiber networks both undergo weakening under cyclic loading [64,65]. Whole

Table 3
Mechanical properties of basement membranes.

Young's modulus	Type of tissue	Method	Comments	Ref
7.5 ± 4.2 kPa	Human corneal basement membrane	AFM		[62]
5.1 ± 1.03 kPa	Human retinal vascular basement membrane	AFM	The stiffness of only the outer surface of the capillary basement membranes was measured	[63]
0.95–3.30 Mpa	Chick retinal basement membrane	AFM	Measured values from embryonic day 4–9. The modulus increases with embryonic development	[55]
3.81–4.07 Mpa	Mouse retinal basement membrane	AFM	Measured values are from neonatal and adult mouse retinal basement membranes. Values increase with increasing age	[55]

arteries, in particular the aorta, stiffen with deformation because of the intrinsic strain stiffening of its filament network [61]. This term refers to a resistance to deformation that increases non-linearly with increasing deformations and is seen in most soft tissues. It stems from the cross-linking of the extracellular matrix, either by covalent bonds or by cross-linking proteins within the tissue [61,66,67].

Another aspect to consider is the residual stresses in the tissue. These stresses refer to stresses that are still present in the absence of actively applied loads and play a role in the macroscopic behavior of blood vessels and heart valves [68,69]. It is possible that these stresses also influence the topography in the micrometer range. Further studies are however needed to elucidate these aspects.

3. Effect of surface topography on endothelium

Many different methods have been used to fabricate surfaces with topographical features that subsequently undergo testing for endothelial cell responses. These methods range from using purely biologically derived materials, to developing matrices by biomimetic approaches, to making highly hierarchical or highly random structures using nano-microfabrication technology. A variety of fabrication techniques are currently used, including self-assembly, electrospinning, lithography, and etching. In this review, substrates that can be categorized as decellularized matrices, electrospun fibers, pillars, pits, or grated surfaces are covered. These structures are commonly studied with endothelial cells, and some allow for a scale-up in fabrication. It would be interesting to also evaluate the endothelial response on small diameter vascular grafts currently available on the market. These grafts are pre-seeded, and many have been tested in clinical trials. However, due to trade secrets, the surface topography is not available in the literature and cannot always be extracted from the clinical trials, therefore they were excluded from this review.

3.1. Decellularized tissues and cell culture-derived matrices

Decellularized tissues and cell-derived matrices hold promise because they approximate the native tissue. In this part, we discuss the current knowledge on how these decellularized and pre-seeded matrices can be prepared and used as a scaffold for the endothelium.

Decellularized matrices isolated from native tissue have similar chemical composition, physical properties, and surface structure as the native vascular basement membranes [71,72]. They are therefore desirable for use as a material for tissue engineering. Decellularized tissues from different species and anatomical origins have been used as a scaffold for endothelial cells. Additionally, in-vitro cell cultures have been decellularized and the matrix used as scaffolds for endothelium

[73]. Vascular matrices have been isolated from a variety of vascular tissues, such as human saphenous vein, human umbilical artery, rat hearts, and porcine aortic valves [71,74–77]. Other sources outside the cardiovascular system include porcine ureters and *in vitro* cell cultures of chondrocytes, preosteoblasts, and fibroblasts [73,78]. Decellularization protocols employ osmotic shock, detergents, proteolytic digestions, and DNase/Rnase treatments. Most methods effectively eliminate the cellular components but show limitations in preserving the ECM structure [79,80]. Limitations of decellularized matrices include remnants of toxic detergents, elicitation of immunoresponses, and a lack of availability, which reduce their suitability for application [81–83]. Side effects due to modifications in the matrix proteins during decellularization could lead to in vivo fibrosis, calcification, and poor endothelialization of the matrix [84].

A review of the field shows that a more systematic research effort will be necessary for overcoming the current limitations associated with native matrices derived from decellularization. For example, very few studies have sought to describe matrix composition or the topographical features in detail before and after decellularization. More often, indirect measures of topographical changes are reported through staining of the main extracellular proteins of the vascular basement membrane, most often collagen or elastin [71,72]. No systematic evaluation of protein structure preservation has been done for matrices used for the endothelium.

Existing literature has relied on two simple readouts to characterize the state of decellularized templates. A first, easily checked metric is the preservation of the overall macroscopic shape of the matrix. For example, whole vascular tissues have been decellularized and reseeded with endothelial cells. One such study showed particularly promising results in which whole rat hearts were decellularized and used as a scaffold for rat aortic endothelial cells [75]. After the decellularization process, the whole matrix kept the original organ's external contour. In the case of cell culture derived matrices, this would require checking how well the thickness, or the volume of the matrix layer is preserved after decellularization. Suitable layer thickness characterization methods include supercritical angle fluorescence microscopy (SAF) and ellipsometry [85]. Nano-indentation can also be used after decellularization as a complementary method.

A second, finer level of quality assessment has been to check for the presence of the major protein components of the matrix post-decellularization. In the same whole rat heart study, collagens I and III, laminin, and fibronectin remained within the structure. Fiber topography and the orientation of the myocardial matrix were also preserved. Both are indicators of a successful decellularization. The whole structure was seeded in a bioreactor by media perfusion. After 7 days, endothelial cells formed single layers in both larger and smaller coronary vessels throughout the heart wall [75]. Translating the advances of pre-seeded matrices into animal experiments have so far shown limited success. Even after the decellularization of porcine pulmonary valves, where collagen and elastin architecture was preserved, few pre-seeded autologous endothelial progenitor cells were present after 1 and 3 months on the matrix when the valve was explanted [72].

In other studies, researchers have developed protocols that preserve collagen IV, the most abundant protein in the vascular basement membrane [38]. In such cases where collagen IV has been preserved but other proteins only partially preserved, the endothelial cells are nevertheless viable, proliferate and are able to form a monolayer after a few days in culture [74,76]. Additionally, the cultured cells are able to synthesize laminin, fibronectin, and chondroitin sulfate (tested for porcine aortic EC seeded on decellularized porcine aortic valves) [76]. It seems that even without complete preservation of the ECM and its elastic fibers, endothelial cells remain viable, can proliferate, and are able to synthesize extracellular proteins [74–76]. Even on a matrices derived from non-vascular origin, the endothelial cells seeded have been shown to proliferate and didn't exhibit any sign of change in morphology [78].

Another category of bio-derived substrates is cell culture-derived matrices. These are matrices decellularized from *in vitro* cell cultures of various cell types. Cell derived matrices from chondrocytes, pre-osteoblasts, and fibroblasts have been characterized and used for human umbilical vein endothelial cells. In this case, the surface roughness from these three matrices was measured over 100 μm × 100 μm areas by AFM and reported to be, respectively, 211 ± 22, 241 ± 24, and 138 ± 5 nm for the different decellularized cultures [73]. Interestingly, the measured roughness was proportional to the measured matrix thickness, which were, respectively, 1200 ± 134, 1700 ± 250, and 860 ± 200 nm. EC morphologies were changed on preosteoblast-derived matrix and fibroblast-derived matrix, showing capillary-like assembly. Endothelial cell morphology on chondrocyte-derived matrix remained unchanged, yet proliferation was higher and cell migration was slower compared to on other cell derived matrices. The different cell behaviors on the different substrates might however be attributed to differences in stiffness rather than topographical differences. The material elasticity measurements revealed Young's moduli of 17.7 ± 4.2 kPa for the chondrocyte-derived matrix, 10.5 ± 1.1 kPa for the preosteoblast-derived matrix and 5.7 ± 0.5 kPa for the fibroblast-derived matrix [73].

Decellularized matrices approximate the complex composition and structure of the native ECM, even though decellularization methods are not optimal. Despite the difficulty in completely preserving the ECM, endothelial cell cultures grown on such substrates are able to form a monolayer, have a morphology similar to that of the native endothelium, and are able to synthesize extracellular matrix proteins. The difficulty in completely preserving the ECM structure is however still an obstacle and involves the risk of fibrosis or stenosis commonly seen after implanting porcine heart valves [86]. More fundamentally, not much is known about the host response [87]. There is still no standard in identifying and validating what important components or structures of the matrix need to be present in the matrix after decellularization. There is also no available information on what potential contaminants must be eliminated except for endotoxins, nucleic acids and extraction aids [87]. In addition, the basic mechanisms of matrix interaction with native tissues remain to be elucidated in order to find which will best serve in each implant.

Decellularized matrices have the potential to exceed any other substrate in performance when it comes to endothelialization and are particularly promising for future applications in medicine. The realization of this full potential hinges on iterative cycles of in-depth characterization and decellularization protocol refinement to yield a template that retains as much as possible the essential part of the original protein diversity, copy number, tertiary and quaternary structures, and spatial distribution within the entire matrix. Newly developed nanoscale analytical methods will prove essential in this endeavor. Superresolution optical methods such as 3D-SAF coupled with immunostaining protocols can, in principle, permit the mapping of protein structure and localization with a precision of ~10 nm in all three axes in a 2D layer with thickness of 1 μm from the glass slide [85]. For thicker matrices, atomic force spectroscopy using cantilevers with antibody-functionalized tips can provide comparable information, though restricted in depth to the top layer of the matrix [88]. In summary, advances in decellularization protocols and more knowledge about the matrix structure and function could lead to a broader use for these substrates.

3.2. Electrospun scaffolds

Under the scanning electron microscope, the native vascular basement membrane appears as a nanofibrous sheet rich in pores. This appearance has inspired the engineering of fibrous substrates for tissue engineering applications, such as endothelializaion. To date, the fabrication of these types of scaffolds has mainly relied on four processing techniques. These are extrusion, self-assembly, phase separation, and electrospinning [89–92]. Among them, electrospinning has emerged as

the most commonly used technique in tissue engineering due to its generality, scalability, and structural similarities to the native ECM [93]. This technique can produce fibrous scaffolds in the nano-to-micro range with tunable fiber and pore sizes. Spun scaffolds are meshes of overlaid fibers with a high surface-area-to-volume ratio and interconnected tortuous pores.

The key geometric parameters defining fibrous scaffolds include the diameter of the fibers, the size of the pores, and how the fibers are aligned. In this review, the effects of these parameters on endothelial response are examined. Most studies on electrospun fibers report the fiber diameter and the pore size, but fewer report topographical features related to fiber density or the roughness of the substrate as a function of the sampling size. These are however important measures of the surface topography for 2D tissue engineering as each cell needs to be supported in the same plane to be able to form junctions with adjacent cells. In the context of fibrous substrates, this means substrates with small pore size are required in order for endothelial cells to form a functional monolayer [94]. In general, the fiber diameter is proportional to the pore size, but post processing can be used to decrease the pore size in order to improve 2D culture conditions for this reason [95]. If the fiber and pore sizes are too large, the cells can infiltrate into the scaffold and the topographical features will direct cells to grow along the fibers [96]. When cells grow along a single fiber in the micrometer range, they have less focal adhesion points, exhibit spindle like morphology [96] and are less likely to form a monolayer.

Endothelial cell responses have been evaluated on electrospun fibers ranging from 100 nm to 20 μm in diameter and pore sizes down to 0.1 μm [95,97–108]. The endothelial responses to these scaffolds are summarized in Table 4.

Two trends emerge from a synthesis of the literature results on the responses of cells to geometric features of fibrous substrates. First, the studies generally show that endothelial response improves when cells are cultured on textured meshes composed of thinner nanofibers and correspondingly smaller pores. Second, it is clear that fiber alignment causes a morphological change of the endothelium, where the cells align along the direction of the aligned fibers. In addition to these geometric effects, all the studies, taken together support the general observation in the field that the nature of the scaffold material can also have a great influence on how well these scaffolds serve as substrates for the endothelium. In general, biologicallyderived, protein-based materials having clear advantages over the purely synthetic ones.

3.2.1. Small fiber and pore size improve the endothelial response

The beneficial effect of surface texturing is manifested in differences in cell responses on fibrous substrates versus on a flat, cast film of the same material. In studies that directly compared electrospun substrates to a cast film, the spun substrates showed more favorable response with HUVECs exhibiting better attachment and higher proliferation compared to on cast film of the same material [95,113].

Not only is the presence of surface texturing important, the spatial frequency of this texturing is also crucial. When electrospun matrices are compared, smaller fiber diameters and pore sizes, corresponding to higher spatial frequencies, improves the endothelial cell response [21, 95,97,98,113,117]. As an example, HUVEC attachment and proliferation is enhanced on smaller fibers when compared to larger fibers of the same material (0.3 and 1.2 μm in diameter vs. 7.0 μm) [97].

3.2.2. Elongated morphology on aligned fibers

When endothelial cell responses on randomly oriented fibers are compared to those on aligned fibers, cells clearly elongate and align in the direction parallel to the fibers [98,107,111,112,114,115]. Cell types tested include bovine aortic endothelial cells, porcine iliac artery endothelial cells, human umbilical cord derived endothelial cells (HUVECs), human outgrowth endothelial cells, and human umbilical vein-derived EA.hy926 endothelial cells [98,107,111–115]. The fiber diameters tested in these studies were in the range of 0.1–8 μm [98,107,

Table 4
Endothelial cell response on electrospun fibers.

Fiber Material	Fiber diameter [μm] / Pore size in ø or area [μm or μm^2] / Fiber alignment	Cell type	Cell response	Ref.
Poly(l-lactide-*co*-ε-caprolactone) made of equimolar poly(l-lactide) and poly(ε-caprolactone)	0.32 ± 0.08 μm 0.2–30 μm- Random-	HUVECs	-Low adhesion. -Low proliferation rate. -Confluency not reached after 1 week. -Elongated morphology.	[97]
Poly(l-lactide-*co*-ε-caprolactone) made of equimolar poly(l-lactide) and poly(ε-caprolactone)	1.16 ± 0.17 μm 0.2–400 μm- Random-	HUVECs	-Low adhesion. -Low proliferation rate. -Confluency not reached after 1 week. -Elongated morphology.	[97]
Poly(l-lactide-*co*-ε-caprolactone) made of equimolar poly(l-lactide) and poly(ε-caprolactone)	7.0 ± 1.0 μm 1–500 μm Random	HUVECs	-Low cell adhesion. -No proliferation in 1 week of culture. -Round morphology.	[97]
Terpolymer containing hexylmethacrylate (HMA), methylmethacrylate (MMA), and methacrylic acid (MAA) in molar ratios of 90:8:2 (referred to as H90)	6 ± 3 μm 270 ± 190 μm^2 Random	HUVECs	-Proliferation and metabolic activity were higher on fibers compared to on cast film of the same material.	[95]
Terpolymer containing HMA, MMA, and MAA (60:38:2 M ratios, referred to as H60)	5 ± 2 μm 690 ± 440 μm^2 Random	HUVECs	-Proliferation and metabolic activity were indistinguishable from those on a cast film and lower than those on tissue culture plastic (TCP).	[95]
Terpolymer containing HMA, MMA, and MAA (20:78:2 M ratios, referred to as H20)	12 ± 12 μm 2200 ± 1400 μm^2 Random	HUVECs	-Proliferation and metabolic activity were indistinguishable from those on a cast film and lower than those on TCP.	[95]
Terpolymer containing HMA, MMA, and MAA (20:78:2 M ratios, referred to as H20)	8.8 ± 2.5 μm NA Aligned	HUVECs	-Cells show elongated morphology as they align along the direction of fibers	[95]
Copolymer of poly(ε-caprolactone) and collagen type I derived from calf skin in 1:1 wt ratio	0.520 ± 0.14 μm 22.7 ± 9.6 μm^2 Random	Bovine carotid artery endothelial cells	-Cell adhesion was better on PCL/collagen scaffold compared to on PCL fibers and on TCP. -No difference in cell proliferation was observed on these three substrates.	[109]
Recombinant human tropoelastin (disuccinimidyl suberate crosslinked)	0.58 ± 0.94 μm 1–6 μm* Random	Porcine bone marrow derived endothelial outgrowth cells	-Good attachment and proliferation. -Confluency reached in 48h of culture. -Cells stained positive for vWF.	[110]
Poly (l-lactic acid)	0.10–0.50 μm 0–3 μm* Random	HUVECs	-Good attachment and proliferation.	[98]
Poly (l-lactic acid)/gelatin (5 %, 10 %, and 20 % gelatin with respect to PLLA weight)	0.10–0.50 μm 0.5 μm* Random	HUVECs	-Cell attachment proportional to gelatin content. More gelatin results in a better attachment.	[98]
Poly (l-lactic acid)/gelatin (5 %, 10 %, and 20 % gelatin with respect to PLLA weight)	0.10–0.50 μm 0–5 μm* Aligned	HUVECs	-Cells orient and elongate along the long axis of the aligned fibers.	[98]
Collagen–chitosan–thermoplastic polyurethane (TPU) blends (glutaraldehyde crosslinked)	0.36 ± 0.22 μm 1–8 μm Random	Porcine iliac artery endothelial cells	-Proliferation better than on TCP	[107]
Collagen–chitosan–thermoplastic polyurethane (TPU) blends (glutaraldehyde crosslinked)	0.26 ± 0.15 μm 1–4 μm Aligned	Porcine iliac artery endothelial cells	-Proliferation better than on TCP -Equally good as on randomly aligned fibers. -Cells slightly oriented along fibers.	[107]
Tecothane (an aromatic polyether polyurethane)	1.20 ± 0.31 μm NA Aligned	Bovine aortic endothelial cells	-Cells align along the fibers within 2h after seeding. -Confluency reached on day 5.	[111]
Tecothane (an aromatic polyether polyurethane)	1.20 ± 0.31 μm NA Aligned	Human umbilical vein-derived EA.hy926 endothelial cells	-Cells align along the fibers within 2h of seeding. -Confluency reached on day 5.	[111]
Fibronectin coated Tecothane (Fibrous substrate containing ridges and grooves. The ridge width, channel width and channel depth were 3.6 ± 0.2, 3.9 ± 0.1 and 0.9 ± 0.03 μm, respectively.)	1–5 μm* NA Random	Bovine aortic endothelial cells	-Cells align along the micron-scale groove pattern on the surface -Good proliferation -Confluency reached on day 5. -The phenotype was confirmed with VE-cadherin staining.	[111]
Fibronectin coated Tecothane (Fibrous substrate containing ridges and grooves. The ridge width, channel width and channel depth were 3.6 ± 0.2, 3.9 ± 0.1 and 0.9 ± 0.03 μm, respectively.)	NA NA Random	Human umbilical vein-derived EA.hy926 endothelial cells	-Cells align along the micron-scale groove pattern on the surface -Good proliferation -Confluency reached on day 5. -The phenotype was confirmed with VE-cadherin staining. -Cells were responsive to the pro-inflammatory cytokine TNF-α, like native endothelium.	[111]
Poly-ε-caprolactone	0.30–0.05 μm 0–8 μm*	Bovine aortic endothelial cells	-Substrate supports cell attachment -oor proliferation rate	[112]

Table 4 (*continued*)

Fiber Material	Fiber diameter [μm] / Pore size in ⌀ or area [μm or μm²] / Fiber alignment	Cell type	Cell response	Ref.
	Random, but on a grated material		-Confluency not reached after 6.5 days	
Poly-ε-caprolactone	0.30–0.50 μm / NA / Aligned	Bovine aortic endothelial cells	-Substrate supports cell attachment -Poor proliferation rate -Cell orient along the aligned fibers.	[112]
Terpolymer containing HMA, MMA, and MAA (20:78:2 M ratios, referred to as H20)	4–12 μm / 0–4000 μm² / Random	human blood outgrowth endothelial cells	-Better adhesion than on align fibers and cast film but not better than on TCP. -Adhesion is better compared to that of HUVECs. -Confluency was not reached by day 9. -Cells express vWF.	[113]
Terpolymer containing HMA, MMA, and MAA (20:78:2 M ratios, referred to as H20)	4–8 μm / 0–2000 μm² / Aligned	human blood outgrowth endothelial cells	-Lower proliferation rate than on random fibers. -Cells express vWF.	[113]
Terpolymer containing HMA, MMA, and MAA (20:78:2 M ratios, referred to as H20)	4–12 μm / 0–4000 μm² / Random	HUVECs	-Attachment and proliferation are higher than on cast film -Attachment and proliferation are worse than on TCP. -Adhesion is better compared to that of HUVECs. -Confluency was not reached by day 9. -Cells express vWF.	[113]
Terpolymer containing HMA, MMA, and MAA (20:78:2 M ratios, referred to as H20)	4–8 μm / 0–2000 μm² / Aligned	HUVECs	-Attachment and proliferation are higher than on cast film -Attachment and proliferation are worse than on TCP. -Attachment and proliferation are worse than on random fibers. -Cells express vWF.	[113]
Poly-L-lactic acid	0.30–0.40 μm / 2–40 μm* / Random	Rabbit outgrowth endothelial (OEC) from peripheral blood	-Better adhesion than on aligned fibers. -Proliferation rate is comparable to on fibronectin-coated culture plates. -Confluency reached on day 3*	[114]
Poly- L-lactic acid	0.30–0.40 μm / 1–25 μm* / Modestly aligned	Rabbit OEC from peripheral blood	-etter proliferation than on random fibers. -Cells align moderately along the fibers.	[114]
Poly-L-lactic acid	0.30–0.40 μm / 0–8 μm* / Highly aligned	Rabbit OEC from peripheral blood	-Better proliferation than on modestly aligned fibers.	[114]
Collagen-coated poly(L-lactic acid)-*co*-poly(epsilon-caprolactone)	0.47 ± 0.08 μm / 6 ± 2 μm / Random	human coronary artery endothelial cells	-Confluency not reached on day 3. -Platelet endothelial cell adhesion molecule-1, fibronectin, and collagen type IV was expressed at the protein level.	[115]
Collagen-coated poly(L-lactic acid)-*co*-poly(epsilon-caprolactone)	0.41 ± 0.13 μm / 0–3 μm* / Aligned	human coronary artery endothelial cells	-Cell alignment along fibers. -Elongated morphology. -Similar protein expression as cells on random fibers	[115]
Polyglycolic acid	0.087 μm / 0.32 μm² / Random	HUVECs	-Proliferation rate is comparable to that on TCP over 5 days.	[116]
Polyglycolic acid with 10 wt% gelatin	0.13 μm / 0.57 μm² / Random	HUVECs	-Proliferation rate is comparable to that on TCP over 5 days.	[116]
Polyglycolic acid with 30 wt% gelatin	0.52 μm / 14 μm² / Random	HUVECs	-Proliferation rate is worse than that on TCP between day 3 and day 5.	[116]
Polyglycolic acid with 50 wt% gelatin	0.86 μm / 20 μm² / Random	HUVECs	-Proliferation rate is worse than that on TCP between day 3 and day 5.	[116]
7.5 % (w/v) silk/Poly (ethylene oxide)	0.38 ± 0.07 μm / 0–3 μm* / Random	Human aortic endothelial cells	-Cobblestone morphology after 1 day, -Network of capillary tubes with lumens from day 4–14. -Cell phenotype confirmed by cell-specific markers: CD146, VE-cadherin, PECAM-1 and vWF.	[94]
Blend of poly(glycerol sebacate) (5 % w/v) and poly(ε-caprolactone) (10 % w/v)	3.4 ± 0.8 μm / 5–50 μm* / Random	GFP-expressing human umbilical vein endothelial cells	-Cells attached and spread along the fiber axis. -Metabolic activity was lower than on aligned fibers. -Cells infiltrated into the scaffold due to large pore size.	[117]

Table 4 (*continued*)

Fiber Material	Fiber diameter [μm] / Pore size in ø or area [μm or μm²] / Fiber alignment	Cell type	Cell response	Ref.
Blend of poly(glycerol sebacate) (5 % w/v) and poly(ε-caprolactone) (10 % w/v)	4.7 ± 0.6 μm 5–30 μm* Aligned	GFP-expressing human umbilical vein endothelial cells	-Cells expressed less CD31 compared to aligned fibers. -The cytoskeleton and the nuclei elongated along the fiber direction. -Metabolic activity is higher than on randomly aligned fibers and cells -Confluency reached on day 7. -Cells infiltrated into the scaffold due to large pore size.	[117]
Type I collagen derived from calf skin and PCL (1:1 wt ratio blends)	0.1 μm 0–2 μm* Random, modestly aligned, and highly aligned	HUVECs	-Coble stone morphology on random fibers but elongated and aligned with the direction of the fibers on modestly and highly aligned fibers -F-actin located parallel to the fibers only on fully aligned scaffolds -VE-cadherin expressed -Higher level of vinculin expressed on aligned fibers -Cells remains better attached to highly aligned fibers when placed under flow -Confluency on day 3	[21]
Type I collagen derived from calf skin and PCL (1:1 wt ratio blends)	0.3 μm 0.5–5 μm* Random, modestly aligned, and highly aligned	HUVECs	-Same response as to 0.1 μm fibers	[21]
Type I collagen derived from calf skin and PCL (1:1 wt ratio blends)	1.2 μm 1–10 μm*- Random, modestly aligned, and highly aligned-	HUVECs	-Round morphology independent of fiber alignment. -Cells infiltrated into the scaffold. -VE-cadherin not expressed -Confluency not reached on day 3	[21]
Polycaprolactone (PCL) and polyethyleneoxide (PEO). Blend of 18 w/v% PCL and 0.6 w/v PEO	4.92 ± 0.23 μm 5–40 μm* Random	HUVECs	-Cell spreading better than on 6 w/v% PCL and 4.2 w/v PEO blend -Cell proliferation better than on pure PCLE fibers and on 6 w/v% PCL and 4.2 w/v PEO blend -Confluency not reached on day 14	[108]
Polycaprolactone (PCL) and polyethyleneoxide (PEO). Blend of 6 w/v% PCL and 4.2 w/v% of PEO	19.63 ± 0.34 μm NA Random	HUVECs	-Proliferation less than on pure PCL fibers -Confluency not reached on day 14	[108]
Polycaprolactone (PCL) followed by different levels of self-induced crystallization	~0.05–1 μm* NA Aligned	HUVECs	-Self-induced crystallization on fibers promotes proliferation -Cells migrate faster on crystallized fibers compared to smooth fibers and less crystalline fibers -More polarized adhesion with a higher nuclear shape index for crystalline fibers	[118]
Polycaprolactone (PCL), and PCLfollowed by self-induced crystallization	0.1-1.5 μm* NA Random and aligned	HUVECs	-Actin polymerization and directional migration regulated through Rac1 and Cdc42 -Elongated morphology	[119]

Notes: * denote values extracted by the authors from SEM images provided in the relevant reference.

111–115]. When placed under flow, HUVECs stay better attached and align more with increasing fiber alignment. Cells exhibit thick bundles of oriented F-actin parallel to the alignment of the fibers, similar to the organization of native ECs in straight artery segments under high shear stress [21]. Additionally, under flow, cells growing on aligned fibers expressed vinculin at a level 2–3 times higher than counterparts growing on randomly aligned fibers [21]. The unidirectional surface topography that aligned fibers provide results in a so-called contact guidance which has been shown to direct the alignment of many cell types, including endothelial cells [120–122]. This elongation was observed in both the

cytoskeleton of the cell and the cell nuclei [114,117].

The effects of alignment on attachment and proliferation are not as clear. Veleva et al. showed that human blood outgrowth endothelial cells and HUVECs possess higher metabolic activity and proliferated more on randomly aligned fibers (5 μm in diameter) compared to aligned fibers (5 μm in diameter) and smooth surfaces [113]. When smaller fiber sizes were studied (below 5 μm), the opposite trend was observed. When ECs were seeded on 300–400 nm fibers, the initial attachment was better than on randomly aligned fibers [114]. However, after longer culture time, cell proliferation was higher on partly or fully

aligned fibers [114,117]. Another study on fibers of similar diameter found no differences in proliferation on random (360 ± 220 nm) vs. aligned fibers (256 ± 145 nm) [107].

3.2.3. Biological material or blends perform better than purely synthetic materials

Among the literature results, the most favorable endothelial response was achieved when biologically derived materials or blends of biological and synthetic material were used [98,107,109,110,116]. The shortest culture time to reach confluency was achieved and reported to be 48 h by both Mckenna et al. and Lee et al., using randomly aligned fibers [109,110]. Both used fiber sizes around 500 nm made of either pure recombinant human tropoelastin or a polymer blend (PCL/collagen) [109,110]. The growth rates reported in these two studies were, however, not compared to those on other topographies of these same biological materials. Therefore, it remains unclear if the small-diameter fibrous nature of the substrate was a confounding geometric contributor to the observed performance.

Even though few studies report results on cellular response after longer culture time and dynamic culture, one study using a blend of PLC/collagen (520 ± 14 nm fibers) demonstrated that endothelial cells still adhered and covered a lumen of a graft after pulsatile flow in a bioreactor for 9 days [123]. The same endothelialized grafts were also able to resist adherence of platelets when exposed to blood for 15 min [123].

In general, ECs grown on electrospun substrates maintain their phenotype. This is confirmed by the expression of endothelial cell-specific markers such as VE-cadherin, vWF, CD31, CD146 or PECAM-1 [94,96,105,111,113,115]. However, two studies reported formation of tubular-like structure when human umbilical vein endothelial cells were cultured on cellulose acetate fibers (1.2 µm in diameter) and aligned poly(glycerol sebacate)-poly(ε-caprolactone) fibers (4.7 µm in diameter) [94,117,124].

There are only a limited number of studies attempting to assess cell seeded electrospun scaffolds in animals, and none has approached clinical trials [125]. Zhou et al. demonstrated a good patency of electrospun PCL/chitosan fibers of electorspun grafts after 3 months of implantation in a canine model. Autologous outgrowth endothelial cells were seeded on fibers with an average diameter of 550 ± 120 nm and average porosity of 85 % ± 4.1 %. The grafts were first cultured statically for 2 days and then for 7 days under pulsatile flow (30 dyn/cm^2) before implantation. The endothelial function was preserved during the in vivo remodeling as cells expressed von Willebrand factor, kinase insert domain receptor and endothelial NO synthase comparable to native carotid artery [126].

Overall, topological features of electrospun substrates, in terms of fiber diameter and pore size, affect attachment, proliferation, and morphology (directionality and alignment) of endothelial cells. The results indicate that aligned electrospun scaffolds with small fiber diameters and small pore size can support endothelial cell function. However, to get more information of the effect of the material and topography it would be beneficial to conduct a single study where the fiber diameter and pore size would be kept constant for different materials while analyzing the cell response. True decoupling can be tricky as when you change the material, you may also change other properties like stiffness. So at least it will have to be measured and maybe things like crosslinking have to be done to ensure identical stiffness while alternating the compositions. True decoupling of ECM to fully understand the effect of topography, the substrate needs to be finely tuned spatially and other topography such as pillars and pits would be more suited to the task. Spun matrices are limited in size as current electrospinning methods do not allow for fabrication of matrices with uniform fiber diameter much lower than 100 nm. The feature sizes in spun matrices are therefore considerably larger than those in the native basement membrane, where the average fiber diameter is around 30 nm [13,39,51]. Fiber diameter of this size has been produced in collagen by

a method that couples hydrodynamic flow with drying, but the generality of the method remains to be explored [127,128]. The spun matrices are also usually made of one material and do therefore not represent well the diversity of proteins found in the native matrix. Adding more of relevant ECM proteins or experimenting with blends of decellularized ECM and electrospun scaffolds could provide important cues needed for improved cellular function. Overall, improving these two important aspects of material selection and decreasing fiber size will open up new possibilities and application of electrospun scaffolds for endothelialization.

3.3. Pillars and pits

The technological push for ever higher data storage densities has led the electronics industry to develop a variety of techniques for patterning 2D surfaces. Direct write, one-step patterning of surfaces with critical feature dimensions well below 5 nm is now routine [129,130]. While many of these techniques rely on serial exposure by electron beam or ion beams, modern production machines are able to handle large enough areas for cell culture experiments in reasonable times. The much faster photolithographic technique can also routinely achieve pillars and wires with diameters in the tens to hundreds of nanometers in combination with other microfabrication techniques [131,132].

With these capabilities in place, bioengineers can now fabricate precisely defined surface patterns to systematically study the effect of their geometrical parameters on cell responses. Surfaces with controllable geometric features in the nanometer range have been used to investigate response of various cell types, including endothelial cells [133]. To date, cylindrical pillars and pits have received the most attention with regard to endothelialization, even though the effect of other shapes like hexagons and pyramid shaped structures have also been reported. This is likely due to the simplicity of fabricating cylindrical structures; they are derived from dot arrays patterned in 2D, followed by deposition or etching steps, which allow for precise control of the height of the pillars or the depth of the holes. Such quantifiable geometric parameters also include the diameter, width, and spacing. Even though surfaces in existing studies are not biomimetic, their precise geometry and reproducibility provides a platform to investigate different aspects of the cellular response. Such studies are essential for a fundamental understanding of the signaling pathways underlying the mechanics of cell-surface interactions. Further studies could aim at decoupling the effect of ECM and topography by coating the substrate with different ECM proteins in a way that does not alter the physical properties of the bulk material.

3.3.1. The effect of size - µm pillars versus nanopillars

Studies examining the impact of pillar size on endothelial cells reveal a clear preference for nanopillars, whereas the use of micrometer-scale pillars yields less favorable results. In one example, Dickinson et al. investigated endothelial cell response to micropillar substrates bearing pillars 1 µm–6 µm in height and spaced at distances between 0.6 and 15 µm. They found that for HUVECs and human endothelial colony-forming cells, the viability was highest on flat substrates and decreased with increasing pillar height (highest on 1 µm pillars and lowest on 8 µm pillars). Cells on flat substrates also spread the most and the spreading decreased with increasing pillar height [134].

Pillars in the nanometer range seem more promising for endothelialization. Dalby et al. investigated nanometrically high pillars of 13, 53 and 95 nm height. HGTFN cell coverage (a human endothelial cell line) was better on all the pillars compared to the flat substrate of similar chemistry [20]. Cells on the 13 nm pits, however, start to form multilayers after 1 week in culture. This unusual and unwanted EC response is thought to be due to overstimulated mechanism that activates cell division. Cells need to spread to enter the DNA replication phase of cell division. Therefore, it may be that with more cells spreading on the surfaces, more cells are entering this phase, and therefore the cells are

more proliferative. Cell morphology was different on the taller nanopillars (95 nm) compared to all the other surfaces, as filopodia interaction was apparent for many cells on that substrate and features within the cells were aligning along the tops of the islands. Much fewer stress fibers were detected on the largest pillars and control compared to the 13 and 53 nm pillars [20]. In 2007, Miller et al. showed that 200 nm poly (lactic-co-glycolic) acid hemispheres increased endothelial cell adhesion when compared to smooth surfaces or hemispheres with 100 or 500 nm diameter [134]. The increase in adhesion seems to be restricted to only solid pillars as hollow nanopillars (70 and 110 nm diameter) lead to poorer adhesion and proliferation compared to flat control. The hollow pillars, however, promote migration more than 4 times, increase the production of collagen 2–3 times per cell and increase elastin production 5–8 times per cell in primary human aortic endothelial cells (HAEC). Furthermore, a significant increase in elastin and soluble collagen production of HAEC was observed with an increase in hollow pillar diameter [135]. Other features like pyramids also showed a similar trend with regard to size effect; micron-scale pyramids reduce response in cell migration compared to nano scaled pyramids and flat control [136].

3.3.2. The effect of density/arrangement of pillars

Beside the sizes of the pillars and pits, their density and distribution also affect the endothelial cell response. In the case of nanopillar density, a study using alumina (Al$_2$O$_3$) pillars showed that nano pillars 20–30 nm in diameter uniformly led to a decrease in cell adhesion and proliferation compared to flat controls. The denser the pillars, the lower the adhesion and proliferation [137]. Le Saux et al. investigated randomly a scattered distribution of crystallographically aligned pyramides (53 ± 12, 390 ± 75 and 1858 ± 637 nm high) and their effect on bovine aortic endothelial cells. Fewer cells adhered to the pyramid topographies compared to flat controls [136].

3.3.3. Pits

When looking at the evidence for the effect of pits, the results are not as clear. McNichols et al. studied the effect of hexagonally packed circular pits with a diameter of approximately 23 ± 4 nm on bovine aortic endothelial cells. The cell density was lower on the porous material compared to the flat control. The nanopits, however, enhanced cell spreading (each cell spread over larger area) at both the early and late phases of the cell growth [138]. Similarly, Miller et al. reported enhanced cell adhesion and proliferation on poly(lactic-*co*-glycolic acid) with random circular nanopits [139]. One study has compared EC growth on pores against electrospun fibers. When a material with circular pores (700 nm in diameter with 5 μm center-to center spacing) was compared with electrospun fibers (3.68 ± 0.57 μm in diameter with 8.85 ± 4.40 μm pores), no difference was found in cell adhesion (HUVECs) after 24 h. However, proliferation was enhanced on the pore cast scaffold and after 14 days only endothelial cells on the porous material reached confluence [140]. These studies suggest that circular pits have some benefits for endothelial growth, but further studies are needed to elucidate the response, especially the dependence on pit size and depth.

In summary, dense circular nanopillars positively influence the adhesion, morphology, and motility of endothelial cells. These substrates are especially advantageous for studying cellular mechanisms and pathways as the features on these surfaces can be accurately controlled and modified one at a time. Still, little is known about what causes cells to respond to nanopillars, but it is possible that the increase in EC adhesion on these surfaces is due to an increase in ECM protein adsorption. This adsorption might lead to change of cell adhesions sites of these proteins probably because of increasing boundaries and surface energy on the surface [141,142]. Carpender et al. found a correlation between increased cell adhesion on nano hemispheres and increased protein adsorption (fibronectin and collagen type IV). In this study, series of poly(lactic-co-glycolic acid) hemispheres were fabricated with diameters of 190, 300, 400, or 950 nm and cell adhesion investigated [143]. However, since there was no consistent correlation found among

the size of the templating features, the heights of surface features, and the surface energy through water contact angle measurements, it is unclear whether topographic differences or uncontrolled sample surface chemical state was the cause for the differences in protein adsorption and subsequent cell attachment.

3.4. Ridges and grooves

While pillars and pores are derived from zero-dimensional features written in the plane, grated surfaces, consisting of ridges or grooves, are derived from one-dimensional features of lines. Such surfaces display in-plane anisotropy and influence the degree of endothelial cell elongation and directional alignment via contact guidance [24,144,145]. The geometric parameters of grated surfaces include the depths, the width, and the spacing between adjacent ridges or grooves. As the endothelial cells align and migrate parallel to the groove axis, the parameters of the grating can be tuned to either enhance or decrease that response [145]. More importantly as recent studies have shown, grated materials are also able to decrease the secretion of various inflammatory cytokines and counteract tumor necrosis factor-α (TNF-α) induced inflammation [24,144]. This property of the grated substrate is particularly promising for translation into medical application where decreasing inflammation is a critical factor for healing.

When the influence of individual parameters of the gratings was investigated, it was found that the degree of alignment increases with channel depth and reaches a maximum with 1 μm-deep channels [120]. This result was obtained in a study testing bovine aortic endothelial cells on fibronectin-coated poly(dimethylsiloxane) gratings with depths of 200 nm, 500 nm, 1 μm, and 5 μm, at a constant spacing of 3.5 μm. F-actin filaments and vinculin at focal adhesions also aligned with the groove direction. Maximum alignment was found in 1 μm-deep channels after 1 h in culture [120]. In this case, it was found that the focal adhesions localized at the edges and on the sidewalls and the cell alignment was maintained at least until the cells reached near confluence. The response of endothelium to align with the gratings is only present on surfaces with dimensions less than 5 μm. Larger features did not cause the elongation of cells and thus induced different focal adhesion localization [120,146].

When other aspects of the grating geometry were investigated, it was found that the width of the grooves had the most pronounced effect on the orientation and alignment when equal to or wider than 400 nm [147]. Also, higher ratios of ridge to groove widths (1:1, 1:2 vs. 1:5) resulted in greater endothelial cell elongation and directional alignment [144].

Aside from alignment, less has been reported about other cell responses on grated material such as adhesion, proliferation, and migration. One paper showed that migration peaked on the 600 nm wide grooves [147]. Only one study reported on the effect on proliferation, but no differences were found between grated and smooth substrates [120]. Cell adhesion, however, increased significantly when grating spacing decreased to the nanometer scale (rat aortic endothelial cells on titanium channels with widths and spacing of 750 nm, 1 μm, 2 μm and 5 μm) [146]. That trend towards better response on nanometric feature sizes is consistent with what has been described in previous chapters on endothelial behavior on pillars, pits, and fibrous materials.

How different endothelial cell types respond to topography is in general not well understood. Only one study has compared the response among different endothelial cell types. This study was on the effect of grated material (300 nm in depth, and 200 nm - 2 μm wide) on orientation/elongation, proliferation, and migration. Of the four tested cell types (HUVECs, dermal microvascular endothelial cells, aortic endothelial cells and saphenous vein endothelial cells), HUVEC cells were unique in proliferating less in response to a decrease in topographic feature size. This result indicates that different endothelial cell types respond differently to topography [147].

One of the most interesting responses of endothelium to grated substrates is the effect on inflammation. Evidence shows that the grated

substrate can cause the endothelium to reduce the secretion of inflammatory cytokines when compared to flat substrate [144]. The link to inflammation has been demonstrated in two studies. In one of them, Uttayarat et al. created a tubular vascular graft based on electrospun fibers textured with ridges and grooves on the inner, lumen side. The fibrous substrate was made from polyurethane. The inner groove patterns were obtained by electrospinning onto a cylindrical mold bearing ridges and channels with the ridge width, channel width, and channel depth being 3.6 ± 0.2, 3.9 ± 0.1 and 0.9 ± 0.03 μm, respectively [111]. In addition to exhibiting an elongated morphology parallel to the micro patterns, the ECs maintained their phenotype and were responsive to stimulation with the pro-inflammatory cytokine TNF-α [111]. As previously mentioned, grated topographies have also been shown to decrease the secretion of inflammatory cytokines. In static culture, gratings of 550 nm ridge width, 600 nm depth and 1.10 μm groove width lowered the secretion of IL-1β, IL-3 and MCP-1, compared to un-patterned substrates [144]. Additionally, grated substrate of depth, ridge and width of 1 μm inhibits NF-kB activation downstream of TNF-α treatment. This anti-inflammatory effect has the potential to contribute to an increased stability of the endothelium in vivo [24]. Finally grated surfaces can be used to obtain confluent endothelium on a synthetic substrate under flow starting from a minimal cell seeding (with only half of the surface area covered with ECs) [70].

Overall, the literature shows that grated materials have an influence on cell alignment and directionality and that it has the potential to counteract TNF-α induced inflammation. Grated materials additionally influence the adhesion and migration of the endothelium but the responses vary among endothelial cell types. The molecular mechanisms mediating these observations remains to be studied.

4. Discussion

From the existing literature on endothelial cells, it is clear that surface topography influencesadhesion, proliferation, morphology, phenotype, as well as influencing cytokine production related to inflammation. Ridges and grooves promote cellular alignment, reaching a peak in 1 μm-deep channels, and can act in an anti-inflammatory way. Aligned fiber also influence morphology and the degree of EC alignment. Overall, nanostructures are more favorable to achieve improved attachment and proliferation compared with microstructures. Beside contact guidance, the underlying mechanisms that cause these cellular effects in general are mostly unknown. Contact guidance is a mechanism where the ECM enforces spatial constraints on the lamellipodia which elongates the shape of the cell and hence enforces migration direction [148]. However, despite the fact that other mechanistic research in these directions is not well known, some hypotheses are emerging. In the next sections, we discuss two pathways, differing by the location with respect to the cell membrane where biochemical signaling starts. The first

pathway is extracellularly-initiated, it begins with the adhesion of extracellular proteins onto substrate surface nanostructures. The aggregation and/or conformational change of these adsorbed proteins, in turn, directs and promotes cellular adhesion, thus triggering cell responses. The second pathway is intracellularly-initiated. Following the physical deformation of the cell membrane as it wraps around surface nanostructures, intracellular curvature sensing and curvature inducing proteins aggregate on the lumen side to trigger down-stream signaling. Conceptually, these two topologically complementary hypotheses span the complete space of possibilities; the cell needs to somehow receive signal from the nanostructured surfaces, either indirectly from molecules located in-between the cell membrane and the surface, or directly from within its own lumen at high-curvature locations (see Fig. 3).

4.1. Protein adhesion

According to the so called "cell adhesion model", cell adhesion to a surface is higher with an increasing number of chemical bonds to that surface [149–151]. An increase in the number of surface bonds can occur via two mechanisms in the context of surface nanostructuring. The first trivial mechanism is an increase in the effective surface area due to increased roughness upon nanostructuring. The second mechanism is a change in the chemical state of the surface, through the intermediacy of altered protein adsorption behavior in the presence of surface nanostructures. Existing studies seem to indicate that the second mechanism is highly relevant under biological conditions. First, it has been well-established in multiple studies that cell-surface bonding is chemically sensitive [152]. Specifically, the attachment of cells to chemically well-defined self-assembled monolayers improves linearly with the hydrophilicity of the monolayer, as reflected by small water contact angles [153]. Second, nanotopographies have been shown to not only affect the conformation and elasticity of the adsorbed proteins [154,155], but to also, more generally, direct the location and patterns of protein adsorption as a function of the size and the shape of these features. Features in the 10–200 nm range seem the most relevant, based on the results of such studies. In general, they support cell attachment, viability, proliferation and thus the time needed to form a monolayer better than substrates with larger features. The relevance of the protein adsorption interlayer is furthermore supported by the observation that nanoscale surface topography does not influence cell adhesion in the absence of serum [143,156]. Even though the characterization of protein-nanostructure interactions is itself in its infancy, due to the complexity of the underlying physical interactions, the general relevance of the process seems highly plausible based on available evidence [153,157,158].
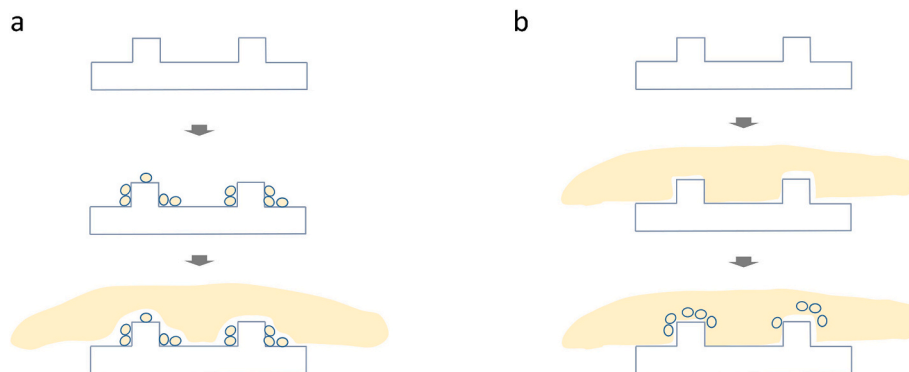

Fig. 3. Mechanistic hypothesis on the underlying mechanisms of nanotopography. a. Extracelluar protein adsorption precedes and directs endothelial attachment. b. Nanotopography mechanically induces cell membrane curvature. This curvature activates downstream signaling.

4.2. Curvature hypothesis

Increasing evidence supports that cell responses to nanotopography are triggered by changes in the curvature of the cell membrane [159]. Recently, a hypothesis named the Curvature Hypothesis was presented by Loue et al., proposing that intracellular proteins in various cell types can recognize membrane curvature induced by features on the underlying substrate [159]. They observed that when the curvature is sufficiently sharp, induced by underlying surface features corresponding to below about 500 nm, these proteins activate downstream signaling pathways that steer the subsequent response of the cell [159,160]. These pathways enhance the process of clathrin-mediated endocytosis and affect actin dynamics [160]. The intracellular proteins involved are clathrin, dynamin-2,four different curvature-sensing proteins, F-BAR protein FCHo1, N-BAR protein amphiphysin 1, and ENTH protein Epsin 1. The curvature of the nuclear membrane might also activate cellular pathways, like chromatin pathways and gene expression [159,161,162]. Even though not demonstrated directly for endothelial cells, it is likely that the underlying mechanisms are similar, as they show some of the same characteristics and activated the response, i.e. the accumulation of actin fibers at the top of the nanopillars [20].

A 3D computation model has been created for cells, however not specific to endothelium, that describes lamellipodium-based motion of cells in arbitrarily shaped and topographically structured surroundings [163]. The model uses curvature and cylindrical confinement and fibers to simulate the cellular effect. The computations showed that confinement, substrate curvature and topography modulate the cell's speed, shape, and actin organization. Furthermore, it was able to effect the direction of motion along axes defined by the constraints [163].

4.3. Conclusion

The various types of structured surfaces that scientists and bioengineers have investigated to date, despite the diversity in materials, structural details, and cell types used, together show several consistent trends. From a practical engineering point of view, the trends we have so far observed from electrospun membrane studies, for example, point to the benefit of going to smaller ECM-inspired fibrous structures, based on biologically derived polymers. Currently available fabrication methods are limited and cannot, as yet, produce a material which approximates
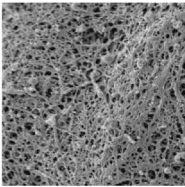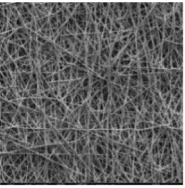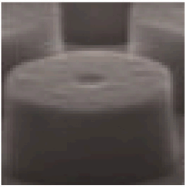

Key aspect for the design of synthetic substrates for EC

Decellularized matrices	**Key concepts** • Matrix that has all the components (proteins, stiffness topography etc.) to serve as a scaffold **Open topics** • Identification and validation of key components and structures that need to be present in the matrix after decellularization ○ Complete preservation of these components • Exploring the use of in vitro grown ECM
Electrospun scaffolds	**Key concepts** • Fiber thickness in nanometer range < 500 nm • Postprocessing to reach structures in < 500 nm • Biological materials or blends over synthetic materials **Open topics** • Implementing materials that include or better represent EC ECM proteins • Decreasing fiber size
Ridges and grooves	**Key concepts** • Cells align along the grooves • Protects EC from inflammation **Open topics** • Other cell responses than morphology needs to be defined • Combination of ridges and grooves with nanostructures • Application in designing structures that are able to expand and contract
Pillars and pits	**Key concepts** • Nanostructures over microstructures **Open topics** • Determining optimal distribution and patterning • Nanofabrication techniques where the geometry can be finely tuned in each dimension are optimal to study the relationship between topography and cells

Fig. 4. Key aspects for the design of substrates for endothelialization. SEM image of decellulaized matrix reprinted with permission from Ref. [39].. Grated substrate. SEM image reprinted with permission from Ref. [70].

the native matrix in material composition, structure, or function. Research efforts might therefore be directed to developing methods to produce such biologically-similar substrates. When looking at decellularized ECM, there is tremendous potential for their use. However, its full potential will only be achieved when all contaminants have been identified and eliminated, and when decellularization protocols have been refined so that all relevant parts for cellular function remain intact. From a fundamental science point of view, the knowledge we have so far is empirical and fragmentary. Studying and understanding the underlying molecular mechanisms in matrix-cell interactions, driven by both intracellular and extracellular responses to topography, will be necessary for the rational design of substrates with the optimal surface properties. Balancing topography-specific responses against other controllable factors (e.g. surface chemistry) will enhance the long-term functionality of the endothelium in medical devices. A summary of key aspects for the design of synthetic substrates for EC can be seen in Fig. 4.

CRediT authorship contribution statement

Oddny Bjorgvinsdottir: Writing – original draft, Conceptualization. **Stephen J. Ferguson:** Writing – review & editing, Supervision, Project administration, Funding acquisition, Conceptualization. **Bergthora Sigridur Snorradottir:** Writing – review & editing, Supervision, Project administration, Conceptualization. **Thorarinn Gudjonsson:** Writing – review & editing, Supervision, Project administration, Conceptualization. **Karin Wuertz-Kozak:** Writing – review & editing, Supervision, Project administration, Funding acquisition, Conceptualization.

Declaration of competing interest

The authors declare that they have no known competing financial interests or personal relationships that could have appeared to influence the work reported in this paper.

Data availability

No data was used for the research described in the article.

Acknowledgements

References

[1] World Health Organization, World heart day 2017, Available, http://www.who.int/cardiovascular_diseases/world-heart-day-2017/en/, 2018.
[2] E.J. Benjamin, et al., Heart disease and stroke statistics-2018 update: a report from the American heart association, Circulation 137 (12) (2018) e67–e492.
[3] P.M. Eckman, R. John, Bleeding and thrombosis in patients with continuous-flow ventricular assist devices, Circulation 125 (24) (2012) 3038–3047.
[4] I.H. Jaffer, J.C. Fredenburgh, J. Hirsh, J.I. Weitz, Medical device-induced thrombosis: what causes it and how can we prevent it? J. Thromb. Haemostasis 13 (Suppl 1) (2015) S72–S81.
[5] R. Biran, D. Pond, Heparin coatings for improving blood compatibility of medical devices, Adv. Drug Deliv. Rev. 112 (2017) 12–23 (in English).
[6] J.W. Yau, H. Teoh, S. Verma, Endothelial cell control of thrombosis, BMC Cardiovasc. Disord. 15 (2015) 130.
[7] J. Iqbal, J. Gunn, P.W. Serruys, Coronary stents: historical development, current status and future directions, Br. Med. Bull. 106 (2013) 193–211.
[8] P. Zilla, D. Bezuidenhout, P. Human, Prosthetic vascular grafts: wrong models, wrong questions and no healing, Biomaterials 28 (34) (Dec 2007) 5009–5027.
[9] R.O. Hynes, The extracellular matrix: not just pretty fibrils, Science 326 (5957) (2009) 1216–1219.
[10] J.A. Eble, S. Niland, The extracellular matrix of blood vessels, Curr. Pharmaceut. Des. 15 (12) (2009) 1385–1400 (in English).
[11] J.A. Wood, S.J. Liliensiek, P. Russell, P.F. Nealey, C.J. Murphy, Biophysical cueing and vascular endothelial cell behavior, Materials 3 (3) (2010) 1620–1639 (in English).
[12] J.Z. Gasiorowski, S.J. Liliensiek, P. Russell, D.A. Stephan, P.F. Nealey, C. J. Murphy, Alterations in gene expression of human vascular endothelial cells associated with nanotopographic cues, Biomaterials 31 (34) (2010) 8882–8888.
[13] S. Brody, T. Anilkumar, S. Liliensiek, J.A. Last, C.J. Murphy, A. Pandit, Characterizing nanoscale topography of the aortic heart valve basement membrane for tissue engineering heart valve scaffold design, Tissue Eng. 12 (2) (2006) 413–421.
[14] R.G. Flemming, C.J. Murphy, G.A. Abrams, S.L. Goodman, P.F. Nealey, Effects of synthetic micro- and nano-structured surfaces on cell behavior, Biomaterials 20 (6) (1999) 573–588.
[15] N.W. Karuri, T.J. Porri, R.M. Albrecht, C.J. Murphy, P.F. Nealey, Nano- and microscale holes modulate cell-substrate adhesion, cytoskeletal organization, and -beta1 integrin localization in SV40 human corneal epithelial cells, IEEE Trans. NanoBioscience 5 (4) (2006) 273–280.
[16] A.I. Teixeira, P.F. Nealey, C.J. Murphy, Responses of human keratocytes to micro- and nanostructured substrates, J. Biomed. Mater. Res. 71a (3) (2004) 369–376 (in English).
[17] S. Heydarkhan-Hagvall, et al., Influence of systematically varied nano-scale topography on cell morphology and adhesion, Cell Commun. Adhes. 14 (5) (2007) 181–194.
[18] C.J. Bettinger, R. Langer, J.T. Borenstein, Engineering substrate topography at the micro- and nanoscale to control cell function, Angew. Chem. Int. Ed. 48 (30) (2009) 5406–5415 (in English).
[19] E.A. Cavalcanti-Adam, D. Aydin, V.C. Hirschfeld-Warneken, J.P. Spatz, Cell adhesion and response to synthetic nanopatterned environments by steering receptor clustering and spatial location, HFSP J. 2 (5) (2008) 276–285.
[20] M.J. Dalby, M.O. Riehle, H. Johnstone, S. Affrossman, A.S. Curtis, In vitro reaction of endothelial cells to polymer demixed nanotopography, Biomaterials 23 (14) (2002) 2945–2954.
[21] B.M. Whited, M.N. Rylander, The influence of electrospun scaffold topography on endothelial cell morphology, alignment, and adhesion in response to fluid flow, Biotechnol. Bioeng. 111 (1) (2014) 184–195.
[22] J.Q. Liang, et al., Endothelial cell morphology regulates inflammatory cells through MicroRNA transferred by extracellular vesicles, Front. Bioeng. Biotechnol. 8 (2020) (in English).
[23] H. Jeon, et al., Combined effects of substrate topography and stiffness on endothelial cytokine and chemokine secretion, ACS Appl. Mater. Interfaces 7 (8) (2015) 4525–4532 (in English).
[24] G. Stefopoulos, C. Giampietro, V. Falk, D. Poulikakos, A. Ferrari, Facile endothelium protection from TNF-alpha inflammatory insult with surface topography, Biomaterials 138 (2017) 131–141.
[25] M. Félétou, The Endothelium, Morgan & Claypool Life Sciences, San Rafael (CA), 2011.
[26] A.I. Lamond, Molecular biology of the cell, 4th edition, Nature 417 (6887) (2002) 383 (in English).
[27] C. Michiels, Endothelial cell functions, J. Cell. Physiol. 196 (3) (2003) 430–443.
[28] A.J. Gale, Continuing education course #2: current understanding of hemostasis, Toxicol. Pathol. 39 (1) (2011) 273–280.
[29] Z. Li, M.K. Delaney, K.A. O'Brien, X. Du, Signaling during platelet adhesion and activation, Arterioscler. Thromb. Vasc. Biol. 30 (12) (2010) 2341–2349.
[30] M. Cicmil, J.M. Thomas, M. Leduc, C. Bon, J.M. Gibbins, Platelet endothelial cell adhesion molecule-1 signaling inhibits the activation of human platelets, Blood 99 (1) (2002) 137–144.
[31] J. Rivera, M.L. Lozano, L. Navarro-Nunez, V. Vicente, Platelet receptors and signaling in the dynamics of thrombus formation, Haematologica-the Hematology Journal 94 (5) (2009) 700–711 (in English).
[32] H. Gray, Anatomy of the Human Body, 20 ed., Lea & Febiger, 1918.
[33] D. Wang, Z. Wang, L. Zhang, Y. Wang, Roles of cells from the arterial vessel wall in atherosclerosis, Mediat. Inflamm. 2017 (2017) 8135934.
[34] M. Ross, W. Pawlina, Kaye Gl. Histology a Text and Atlas, Lippincott Williams & Wilkins, Philadelphia, 2011.
[35] A.S. Faqi, A Comprehensive Guide to Toxicology in Preclinical Drug Development, first ed., Academic Press, London ; Waltham, MA, 2013 pp. xvi, 885.
[36] K. Shipman, Clinical biochemistry: metabolic and clinical aspects, 3rd edition, Ann. Clin. Biochem. 52 (2) (2015) 303–304 (in English).
[37] M.R. Hayden, J.R. Sowers, S.C. Tyagi, The central role of vascular extracellular matrix and basement membrane remodeling in metabolic syndrome and type 2 diabetes: the matrix preloaded, Cardiovasc. Diabetol. 4 (2005) 9.
[38] R. Kalluri, Basement membranes: structure, assembly and role in tumour angiogenesis, Nat. Rev. Cancer 3 (6) (2003) 422–433.
[39] S.J. Liliensiek, P. Nealey, C.J. Murphy, Characterization of endothelial basement membrane nanotopography in rhesus macaque as a guide for vessel tissue engineering, Tissue Eng. 15 (9) (2009) 2643–2651.
[40] M. Frieser, et al., Cloning of the mouse laminin alpha 4 cDNA. Expression in a subset of endothelium, Eur. J. Biochem. 246 (3) (1997) 727–735.
[41] L.M. Sorokin, F. Pausch, M. Frieser, S. Kroger, E. Ohage, R. Deutzmann, Developmental regulation of the laminin alpha5 chain suggests a role in epithelial and endothelial cell maturation, Dev. Biol. 189 (2) (1997) 285–300.
[42] F.T. Bosman, I. Stamenkovic, Functional structure and composition of the extracellular matrix, J. Pathol. 200 (4) (Jul 2003) 423–428.
[43] C.M. Kelleher, S.E. McLean, R.P. Mecham, Vascular extracellular matrix and aortic development, Curr. Top. Dev. Biol. 62 (2004) 153–188.

[44] M. Paulsson, Basement-membrane proteins - structure, assembly, and cellular interactions, Crit. Rev. Biochem. Mol. Biol. 27 (1–2) (1992) 93–127 (in English).

[45] J.C. Schittny, P.D. Yurchenco, Basement membranes: molecular organization and function in development and disease, Curr. Opin. Cell Biol. 1 (5) (1989) 983–988 (in English).

[46] P.D. Yurchenco, J.C. Schittny, Molecular architecture of basement-membranes, Faseb. J. 4 (6) (1990) 1577–1590 (in English).

[47] P.D. Yurchenco, S. Smirnov, T. Mathus, Analysis of basement membrane self-assembly and cellular interactions with native and recombinant glycoproteins, Methods Cell Biol. 69 (2002) 111–144.

[48] L.W. Welling, M.T. Zupka, D.J. Welling, Mechanical-properties of basement-membrane, News Physiol. Sci. 10 (1995) 30–35 (in English).

[49] A.I.T. George, A. Abrams, Paul F. Nealey, Christopher J. Murphy, A.L. Angela Dillow (Eds.), Biomimetic Materials and Design. Biointerfacial Strategies, Tissue Engineering and Targeted Drug Delivery, first ed. ed., 2002. Boca Raton.

[50] A.J. Ridley, A. Hall, The small gtp-binding protein Rho regulates the assembly of focal adhesions and actin stress fibers in response to growth-factors, Cell 70 (3) (1992) 389–399 (in English).

[51] G.A. Abrams, S.S. Schaus, S.L. Goodman, P.F. Nealey, C.J. Murphy, Nanoscale topography of the corneal epithelial basement membrane and Descemet's membrane of the human, Cornea 19 (1) (2000) 57–64.

[52] Y.P. Xi, E.G. Nette, D.W. King, M. Rosen, Age-related changes in normal human basement membrane, Mech. Ageing Dev. 19 (4) (1982) 315–324.

[53] R. Vracko, E.P. Benditt, Capillary basal lamina thickening. Its relationship to endothelial cell death and replacement, J. Cell Biol. 47 (1) (1970) 281–285.

[54] R. Vracko, D. Thorning, T.W. Huang, Basal lamina of alveolar epithelium and capillaries - quantitative changes with aging and in diabetes-mellitus, Am. Rev. Respir. Dis. 120 (5) (1979) 973–983 (in English).

[55] J. Candiello, et al., Biomechanical properties of native basement membranes, FEBS J. 274 (11) (2007) 2897–2908.

[56] J.G. Jacot, S. Dianis, J. Schnall, J.Y. Wong, A simple microindentation technique for mapping the microscale compliance of soft hydrated materials and tissues, J. Biomed. Mater. Res. 79 (3) (2006) 485–494.

[57] D.M. Ebenstein, L.A. Pruitt, Nanoindentation of soft hydrated materials for application to vascular tissues, J. Biomed. Mater. Res. 69 (2) (2004) 222–232.

[58] T. Oie, et al., Local elasticity imaging of vascular tissues using a tactile mapping system, J. Artif. Organs 12 (1) (2009) 40–46 (in English).

[59] A. Lundkvist, E. Lilleodden, W. Siekhaus, J. Kinney, L. Pruitt, M. Balooch, Viscoelastic Properties of Healthy Human Artery Measured in Saline Solution by AFM-Based Indentation Technique, in: Thin Films: Stresses and Mechanical Properties Vi, vol. 436, 1997, pp. 353–358 (in English).

[60] A.J. Engler, L. Richert, J.Y. Wong, C. Picart, D.E. Discher, Surface probe measurements of the elasticity of sectioned tissue, thin gels and polyelectrolyte multilayer films: correlations between substrate stiffness and cell adhesion, Surf. Sci. 570 (1–2) (2004) 142–154 (in English).

[61] R.T. Miller, Mechanical properties of basement membrane in health and disease, Matrix Biol. 57–58 (2017) 366–373.

[62] J.A. Last, S.J. Liliensiek, P.F. Nealey, C.J. Murphy, Determining the mechanical properties of human corneal basement membranes with atomic force microscopy, J. Struct. Biol. 167 (1) (2009) 19–24.

[63] W. Halfter, et al., Diabetes-related changes in the protein composition and the biomechanical properties of human retinal vascular basement membranes, PLoS One 12 (12) (2017) e0189857.

[64] S. Munster, L.M. Jawerth, B.A. Leslie, J.I. Weitz, B. Fabry, D.A. Weitz, Strain history dependence of the nonlinear stress response of fibrin and collagen networks, Proc. Natl. Acad. Sci. U. S. A. 110 (30) (2013) 12197–12202.

[65] N.A. Kurniawan, L.H. Wong, R. Rajagopalan, Early stiffening and softening of collagen: interplay of deformation mechanisms in biopolymer networks, Biomacromolecules 13 (3) (2012) 691–698.

[66] J.D. Humphrey, E.R. Dufresne, M.A. Schwartz, Mechanotransduction and extracellular matrix homeostasis, Nat. Rev. Mol. Cell Biol. 15 (12) (2014) 802–812.

[67] G. Zagar, P.R. Onck, E. van der Giessen, Two fundamental mechanisms govern the stiffening of cross-linked networks, Biophys. J. 108 (6) (2015) 1470–1479.

[68] E.E. van Haaften, C.V.C. Bouten, N.A. Kurniawan, Vascular mechanobiology: towards control of in situ regeneration, Cells 6 (3) (2017).

[69] M. Genet, et al., Heterogeneous growth-induced prestrain in the heart, J. Biomech. 48 (10) (2015) 2080–2089.

[70] G. Stefopoulos, F. Robotti, V. Falk, D. Poulikakos, A. Ferrari, Endothelialization of rationally microtextured surfaces with minimal cell seeding under flow, Small 12 (30) (2016) 4113–4126.

[71] P.J. Schaner, et al., Decellularized vein as a potential scaffold for vascular tissue engineering, J. Vasc. Surg. 40 (1) (2004) 146–153 (in English).

[72] J.E. Jordan, J.K. Williams, S.J. Lee, D. Raghavan, A. Atala, J.J. Yoo, Bioengineered self-seeding heart valves, J. Thorac. Cardiovasc. Surg. 143 (1) (2012) 201–208.

[73] P. Du, R. Subbiah, J.H. Park, K. Park, Vascular morphogenesis of human umbilical vein endothelial cells on cell-derived macromolecular matrix microenvironment, Tissue Eng. 20 (17–18) (2014) 2365–2377.

[74] L.Q. Gui, A. Muto, S.A. Chan, C.K. Breuer, L.E. Niklason, Development of decellularized human umbilical arteries as small-diameter vascular grafts, Tissue Eng. 15 (9) (2009) 2665–2676 (in English).

[75] H.C. Ott, et al., Perfusion-decellularized matrix: using nature's platform to engineer a bioartificial heart, Nat. Med. 14 (2) (2008) 213–221 (in English).

[76] R.W. Grauss, M.G. Hazekamp, F. Oppenhuizen, C.J. van Munsteren, A. C. Gittenberger-de Groot, M.C. DeRuiter, Histological evaluation of decellularised

porcine aortic valves: matrix changes due to different decellularisation methods, Eur. J. Cardio. Thorac. Surg. 27 (4) (2005) 566–571 (in English).

[77] V. Kumar Kuna, B. Xu, S. Sumitran-Holgersson, Decellularization and recellularization methodology for human saphenous veins, J. Vis. Exp. 137 (2018).

[78] C. Derham, et al., Tissue engineering small-diameter vascular grafts: preparation of a biocompatible porcine ureteric scaffold, Tissue Eng. 14 (11) (2008) 1871–1882.

[79] S. Xu, et al., Preparation and characterization of small-diameter decellularized scaffolds for vascular tissue engineering in an animal model, Biomed. Eng. Online 16 (1) (2017) 55.

[80] G. Goissis, S. Suzigan, D.R. Parreira, J.V. Maniglia, D.M. Braile, S. Raymundo, Preparation and characterization of collagen-elastin matrices from blood vessels intended as small diameter vascular grafts, Artif. Organs 24 (3) (2000) 217–223.

[81] F. Moroni, T. Mirabella, Decellularized matrices for cardiovascular tissue engineering, Am J Stem Cells 3 (1) (2014) 1–20.

[82] T.L. Adair-Kirk, R.M. Senior, Fragments of extracellular matrix as mediators of inflammation, Int. J. Biochem. Cell Biol. 40 (6–7) (2008) 1101–1110 (in English).

[83] E. Rieder, et al., Decellularization protocols of porcine heart valves differ importantly in efficiency of cell removal and susceptibility of the matrix to recellularization with human vascular cells, J. Thorac. Cardiovasc. Surg. 127 (2) (2004) 399–405.

[84] O.F. Khan, M.V. Sefton, Endothelialized biomaterials for tissue engineering applications in vivo, Trends Biotechnol. 29 (8) (2011) 379–387.

[85] C.M. Winterflood, T. Ruckstuhl, D. Verdes, S. Seeger, Nanometer axial resolution by three-dimensional supercritical angle fluorescence microscopy, Phys. Rev. Lett. 105 (10) (2010) 108103.

[86] F.J. Schoen, R.J. Levy, Calcification of tissue heart valve substitutes: progress toward understanding and prevention, Ann. Thorac. Surg. 79 (3) (2005) 1072–1080.

[87] J.M. Aamodt, D.W. Grainger, Extracellular matrix-based biomaterial scaffolds and the host response, Biomaterials 86 (2016) 68–82.

[88] Y.F. Dufrene, D. Martinez-Martin, I. Medalsy, D. Alsteens, D.J. Muller, Multiparametric imaging of biological systems by force-distance curve-based AFM, Nat. Methods 10 (9) (2013) 847–854.

[89] K. Jayaraman, M. Kotaki, Y. Zhang, X. Mo, S. Ramakrishna, Recent advances in polymer nanofibers, J. Nanosci. Nanotechnol. 4 (1–2) (2004) 52–65.

[90] L.A. Smith, P.X. Ma, Nano-fibrous scaffolds for tissue engineering, Colloids Surf. B Biointerfaces 39 (3) (2004) 125–131.

[91] Z.W. Ma, M. Kotaki, R. Inai, S. Ramakrishna, Potential of nanofiber matrix as tissue-engineering scaffolds, Tissue Eng. 11 (1–2) (2005) 101–109 (in English).

[92] R.E. Unger, K. Peters, Q. Huang, A. Funk, D. Paul, C.J. Kirkpatrick, Vascularization and gene regulation of human endothelial cells growing on porous polyethersulfone (PES) hollow fiber membranes, Biomaterials 26 (17) (2005) 3461–3469.

[93] S.G. Kumbar, R. James, S.P. Nukavarapu, C.T. Laurencin, Electrospun nanofiber scaffolds: engineering soft tissues, Biomed. Mater. 3 (3) (2008) 034002.

[94] X. Zhang, C.B. Baughman, D.L. Kaplan, In vitro evaluation of electrospun silk fibroin scaffolds for vascular cell growth, Biomaterials 29 (14) (2008) 2217–2227.

[95] D.E. Heath, J.J. Lannutti, S.L. Cooper, Electrospun scaffold topography affects endothelial cell proliferation, metabolic activity, and morphology, J. Biomed. Mater. Res. 94 (4) (2010) 1195–1204.

[96] Y.M. Ju, J.S. Choi, A. Atala, J.J. Yoo, S.J. Lee, Bilayered scaffold for engineering cellularized blood vessels, Biomaterials 31 (15) (2010) 4313–4321 (in English).

[97] I.K. Kwon, S. Kidoaki, T. Matsuda, Electrospun nano- to microfiber fabrics made of biodegradable copolyesters: structural characteristics, mechanical properties and cell adhesion potential, Biomaterials 26 (18) (2005) 3929–3939 (in English).

[98] K.T. Shalumon, S. Deepthi, M.S. Anupama, S.V. Nair, R. Jayakumar, K. P. Chennazhi, Fabrication of poly (L-lactic acid)/gelatin composite tubular scaffolds for vascular tissue engineering, Int. J. Biol. Macromol. 72 (2015) 1048–1055 (in English).

[99] T.H. Nguyen, A.R. Padalhin, H.S. Seo, B.T. Lee, A hybrid electrospun PU/PCL scaffold satisfied the requirements of blood vessel prosthesis in terms of mechanical properties, pore size, and biocompatibility, J. Biomater. Sci. Polym. Ed. 24 (14) (2013) 1692–1706.

[100] S.D. Wang, Y.Z. Zhang, G.B. Yin, H.W. Wang, Z.H. Dong, Electrospun polylactide/silk fibroin-gelatin composite tubular scaffolds for small-diameter tissue engineering blood vessels, J. Appl. Polym. Sci. 113 (4) (2009) 2675–2682 (in English).

[101] S. Wang, Y. Zhang, H. Wang, G. Yin, Z. Dong, Fabrication and properties of the electrospun polylactide/silk fibroin-gelatin composite tubular scaffold, Biomacromolecules 10 (8) (2009) 2240–2244.

[102] S.J. Lee, J.J. Yoo, G.J. Lim, A. Atala, J. Stitzel, In vitro evaluation of electrospun nanofiber scaffolds for vascular graft application, J. Biomed. Mater. Res. 83 (4) (2007) 999–1008.

[103] C.Y. Xu, R. Inai, M. Kotaki, S. Ramakrishna, Electrospun nanofiber fabrication as synthetic extracellular matrix and its potential for vascular tissue engineering, Tissue Eng. 10 (7–8) (2004) 1160–1168 (in English).

[104] J. Stitzel, et al., Controlled fabrication of a biological vascular substitute, Biomaterials 27 (7) (2006) 1088–1094.

[105] W. He, et al., Tubular nanofiber scaffolds for tissue engineered small-diameter vascular grafts, J. Biomed. Mater. Res. 90 (1) (2009) 205–216.

[106] A.M. Nicolini, T.D. Toth, J.Y. Yoon, Tuneable nanoparticle-nanofiber composite substrate for improved cellular adhesion, Colloids Surf. B Biointerfaces 145 (2016) 830–838.

[107] C. Huang, R. Chen, Q.F. Ke, Y. Morsi, K.H. Zhang, X.M. Mo, Electrospun collagen-chitosan-TPU nanofibrous scaffolds for tissue engineered tubular grafts, Colloids Surf. B Biointerfaces 82 (2) (2011) 307–315 (in English).

[108] M.B. Taskin, D. Xia, F. Besenbacher, M.D. Dong, M.L. Chen, Nanotopography featured polycaprolactone/polyethyleneoxide microfibers modulate endothelial cell response, Nanoscale 9 (26) (2017) 9218–9229 (in English).

[109] S.J. Lee, J. Liu, S.H. Oh, S. Soker, A. Atala, J.J. Yoo, Development of a composite vascular scaffolding system that withstands physiological vascular conditions, Biomaterials 29 (19) (2008) 2891–2898 (in English).

[110] K.A. McKenna, et al., Mechanical property characterization of electrospun recombinant human tropoelastin for vascular graft biomaterials, Acta Biomater. 8 (1) (2012) 225–233.

[111] P. Uttayarat, et al., Micropatterning of three-dimensional electrospun polyurethane vascular grafts, Acta Biomater. 6 (11) (2010) 4229–4237.

[112] H. Wu, J. Fan, C.C. Chu, J. Wu, Electrospinning of small diameter 3-D nanofibrous tubular scaffolds with controllable nanofiber orientations for vascular grafts, J. Mater. Sci. Mater. Med. 21 (12) (2010) 3207–3215.

[113] N. Veleva, et al., Interactions between endothelial cells and electrospun methacrylic terpolymer fibers for engineered vascular replacements, J. Biomed. Mater. Res. 91 (4) (2009) 1131–1139.

[114] H. Lu, Z. Feng, Z. Gu, C. Liu, Growth of outgrowth endothelial cells on aligned PLLA nanofibrous scaffolds, J. Mater. Sci. Mater. Med. 20 (9) (2009) 1937–1944.

[115] W. He, T. Yong, Z.W. Ma, R. Inai, W.E. Teo, S. Ramakrishna, Biodegradable polymer nanofiber mesh to maintain functions of endothelial cells, Tissue Eng. 12 (9) (2006) 2457–2466.

[116] H. Hajiali, S. Shahgasempour, M.R. Naimi-Jamal, H. Peirovi, Electrospun PGA/gelatin nanofibrous scaffolds and their potential application in vascular tissue engineering, Int. J. Nanomed. 6 (2011) 2133–2141.

[117] A.K. Gaharwar, M. Nikkhah, S. Sant, A. Khademhosseini, Anisotropic poly (glycerol sebacate)-poly (-caprolactone) electrospun fibers promote endothelial cell guidance, Biofabrication 7 (1) (2014) 015001.

[118] X. Guo, et al., Endothelial cell migration on poly(epsilon-caprolactone) nanofibers coated with a nanohybrid shish-kebab structure mimicking collagen fibrils, Biomacromolecules 21 (3) (2020) 1202–1213.

[119] Y. Zhang, et al., Endothelial cell migration regulated by surface topography of poly(epsilon-caprolactone) nanofibers, ACS Biomater. Sci. Eng. 7 (10) (2021) 4959–4970.

[120] P. Uttayarat, G.K. Toworfe, F. Dietrich, P.I. Lelkes, R.J. Composto, Topographic guidance of endothelial cells on silicone surfaces with micro- to nanogrooves: orientation of actin filaments and focal adhesions, J. Biomed. Mater. Res. 75 (3) (2005) 668–680.

[121] E.T. den Braber, J.E. de Ruijter, L.A. Ginsel, A.F. von Recum, J.A. Jansen, Orientation of ECM protein deposition, fibroblast cytoskeleton, and attachment complex components on silicone microgrooved surfaces, J. Biomed. Mater. Res. 40 (2) (1998) 291–300.

[122] C. Oakley, D.M. Brunette, Topographic compensation: guidance and directed locomotion of fibroblasts on grooved micromachined substrata in the absence of microtubules, Cell Motil Cytoskeleton 31 (1) (1995) 45–58.

[123] B.W. Tillman, S.K. Yazdani, S.J. Lee, R.L. Geary, A. Atala, J.J. Yoo, The in vivo stability of electrospun polycaprolactone-collagen scaffolds in vascular reconstruction, Biomaterials 30 (4) (2009) 583–588.

[124] D. Han, S. Goldgraben, M.D. Frame, P.I. Gouma, A novel nanofiber scaffold by electrospinning and its utility in microvascular tissue engineering, Nanoscale Materials Science in Biology and Medicine 845 (2005) 363–368 (in English).

[125] A. Hasan, Electrospun scaffolds for tissue engineering of vascular grafts, Acta Biomater. 10 (1) (2014) 11–25.

[126] M. Zhou, Development and in vivo evaluation of small-diameter vascular grafts engineered by outgrowth endothelial cells and electrospun chitosan/poly(epsilon-caprolactone) nanofibrous scaffolds, Tissue Eng. 20 (1–2) (2014) 79–91.

[127] J.E. Kirkwood, G.G. Fuller, Liquid crystalline collagen: a self-assembled morphology for the orientation of mammalian cells, Langmuir 25 (5) (2009) 3200–3206.

[128] N.F. Huang, et al., The modulation of endothelial cell morphology, function, and survival using anisotropic nanofibrillar collagen scaffolds, Biomaterials 34 (16) (2013) 4038–4047 (in English).

[129] A. Elsukova, A. Han, D. Zhao, M. Beleggia, Effect of molecular weight on the feature size in organic ice resists, Nano Lett. (2018).

[130] V.R. Manfrinato, et al., Aberration-corrected electron beam lithography at the one nanometer length scale, Nano Lett. 17 (8) (2017) 4562–4567.

[131] Y.K. Choi, J. Zhu, J. Grunes, J. Bokor, G.A. Somorjai, Fabrication of sub-10-nm silicon nanowire arrays by size reduction lithography, J. Phys. Chem. B 107 (15) (2003) 3340–3343 (in English).

[132] Y. Pan, C. Miller, K. Trepka, Y. Tao, Wafer-scale photolithography of ultra-sensitive nanocantilever force sensors, Appl. Phys. Lett. 113 (8) (2018) (in English).

[133] H. Chen, N. Tang, M. Chen, D. Chen, Endothelialization of TiO2 nanorods coated with ultrathin amorphous carbon films, Nanoscale Res. Lett. 11 (1) (2016) 145.

[134] D.C. Miller, K.M. Haberstroh, T.J. Webster, PLGA nanometer surface features manipulate fibronectin interactions for improved vascular cell adhesion, J. Biomed. Mater. Res. 81 (3) (2007) 678–684.

[135] P.P. Lee, T.A. Desai, Nitinol-based nanotubular arrays with controlled diameters upregulate human vascular cell ECM production, ACS Biomater. Sci. Eng. 2 (3) (2016) 409–414.

[136] G. Le Saux, A. Magenau, T. Bocking, K. Gaus, J.J. Gooding, The relative importance of topography and RGD ligand density for endothelial cell adhesion, PLoS One 6 (7) (2011) e21869.

[137] C. Aktas, et al., Micro- and nanostructured Al2O3 surfaces for controlled vascular endothelial and smooth muscle cell adhesion and proliferation, Mater. Sci. Eng., C 32 (5) (2012) 1017–1024 (in English).

[138] C. McNichols, J. Wilkins, A. Kubota, Y.T. Shiu, S.M. Aouadi, P. Kohli, Investigating surface topology and cyclic-RGD peptide functionalization on vascular endothelialization, J. Biomed. Mater. Res. 102 (2) (2014) 532–539.

[139] D.C. Miller, A. Thapa, K.M. Haberstroh, T.J. Webster, Endothelial and vascular smooth muscle cell function on poly(lactic-co-glycolic acid) with nano-structured surface features, Biomaterials 25 (1) (2004) 53–61.

[140] K.J. McHugh, S.L. Tao, M. Saint-Geniez, A novel porous scaffold fabrication technique for epithelial and endothelial tissue engineering, J. Mater. Sci. Mater. Med. 24 (7) (2013) 1659–1670.

[141] D. Khang, J. Carpenter, Y.W. Chun, R. Pareta, T.J. Webster, Nanotechnology for regenerative medicine, Biomed. Microdevices 12 (4) (2010) 575–587.

[142] P. Kim, et al., Fabrication of nanostructures of polyethylene glycol for applications to protein adsorption and cell adhesion, Nanotechnology 16 (10) (2005) 2420–2426.

[143] J. Carpenter, D. Khang, T.J. Webster, Nanometer polymer surface features: the influence on surface energy, protein adsorption and endothelial cell adhesion, Nanotechnology 19 (50) (2008) 505103.

[144] H. Jeon, et al., Combined effects of substrate topography and stiffness on endothelial cytokine and chemokine secretion, ACS Appl. Mater. Interfaces 7 (8) (2015) 4525–4532.

[145] A.M. Greiner, A. Sales, H. Chen, S.A. Biela, D. Kaufmann, R. Kemkemer, Nano- and microstructured materials for in vitro studies of the physiology of vascular cells, Beilstein J. Nanotechnol. 7 (2016) 1620–1641.

[146] J. Lu, M.P. Rao, N.C. MacDonald, D. Khang, T.J. Webster, Improved endothelial cell adhesion and proliferation on patterned titanium surfaces with rationally designed, micrometer to nanometer features, Acta Biomater. 4 (1) (2008) 192–201.

[147] S.J. Liliensiek, J.A. Wood, J. Yong, R. Auerbach, P.F. Nealey, C.J. Murphy, Modulation of human vascular endothelial cell behaviors by nanotopographic cues, Biomaterials 31 (20) (2010) 5418–5426.

[148] G.R. Ramirez-San Juan, P.W. Oakes, M.L. Gardel, Contact guidance requires spatial control of leading-edge protrusion, Mol. Biol. Cell 28 (8) (2017) 1043–1053.

[149] A.A. Khalili, M.R. Ahmad, A review of cell adhesion studies for biomedical and biological applications, Int. J. Mol. Sci. 16 (8) (2015) 18149–18184.

[150] M. Dembo, D.C. Torney, K. Saxman, D. Hammer, The reaction-limited kinetics of membrane-to-surface adhesion and detachment, Proceedings of the Royal Society Series B-Biological Sciences 234 (1274) (1988) 55–83 (in English).

[151] Y.J. Shen, M. Nakajima, S. Kojima, M. Homma, M. Kojima, T. Fukuda, Single cell adhesion force measurement for cell viability identification using an AFM cantilever-based micro putter (in English), Meas. Sci. Technol. 22 (11) (2011).

[152] C.A. Custódio, J.F. Mano, Cell surface engineering to control cellular interactions, Chemnanomat 2 (5) (2016) 376–384 (in English).

[153] Y. Arima, H. Iwata, Effect of wettability and surface functional groups on protein adsorption and cell adhesion using well-defined mixed self-assembled monolayers, Biomaterials 28 (20) (2007) 3074–3082 (in English).

[154] A. Karakecili, G.M.L. Messina, M.C. Yurtsever, M. Gumusderelioglu, G. Marletta, Impact of selective fibronectin nanoconfinement on human dental pulp stem cells, Colloids Surf. B Biointerfaces 123 (2014) 39–48 (in English).

[155] H. Wang, P. Akcora, Confinement effect on the structure and elasticity of proteins interfacing polymers, Soft Matter 13 (8) (2017) 1561–1568.

[156] J.Y. Lim, J.C. Hansen, C.A. Siedlecki, J. Runt, H.J. Donahue, Human foetal osteoblastic cell response to polymer-demixed nanotopographic interfaces, J. R. Soc. Interface 2 (2) (2005) 97–108 (in English).

[157] D.A.P. Kay, C. Dee, Rena Bizios, An Introduction to Tissue-Biomaterial Interactions, Wiley, 2002.

[158] D. Bhattacharyya, H. Xu, R.R. Deshmukh, R.B. Timmons, K.T. Nguyen, Surface chemistry and polymer film thickness effects on endothelial cell adhesion and proliferation, J. Biomed. Mater. Res. 94a (2) (2010) 640–648 (in English).

[159] H.Y. Lou, W. Zhao, Y. Zeng, B. Cui, The role of membrane curvature in nanoscale topography-induced intracellular signaling, Acc. Chem. Res. 51 (5) (2018) 1046–1053.

[160] W.T. Zhao, et al., Nanoscale manipulation of membrane curvature for probing endocytosis in live cells, Nat. Nanotechnol. 12 (8) (2017) 750 (in English).

[161] H. Persson, et al., Fibroblasts cultured on nanowires exhibit low motility, impaired cell division, and DNA damage, Small 9 (23) (2013) 4006–4016 (in English).

[162] F. Badique, et al., Directing nuclear deformation on micropillared surfaces by substrate geometry and cytoskeleton organization, Biomaterials 34 (12) (2013) 2991–3001 (in English).

[163] B. Winkler, I.S. Aranson, F. Ziebert, Confinement and substrate topography control cell migration in a 3D computational model, Commun. Phys. 2 (2019) (in English).

[164] Seung-Hyouk Hong, Ju-Hyung Yun, Hyeong-Ho Park, Joondong Kim; Nanodome-patterned transparent conductor for highly responsive photoelectric device. Appl. Phys. Lett. 7 October 2013; 103 (15): 153504. https://doi.org/10.1063/1.4824688.